IDŐJÁRÁS

QUARTERLY JOURNAL
OF THE HUNGARIAN METEOROLOGICAL SERVICE

CONTENTS

VOL. 97 * NO. 1 * JANUARY–MARCH 1993

IDŐJÁRÁS

Quarterly Journal of the Hungarian Meteorological Service

Editor-in-Chief
E. MÉSZÁROS

Editor
T. TÄNCZER

Technical Editor
Mrs. M. ANTAL

Editorial Office: P.O. Box 39, H–1675 Budapest

Subscription from customers in Hungary should be sent to the Financial Department of the Hungarian Meteorological Service Kitaibel Pál u. 1, 1024 Budapest. The subscription rate is HUF 2000.

Abroad the journal can be purchased from the distributor: KULTURA, P.O. Box 149, H–1389 Budapest. The annual subscription rate is USD 56.

IDŐJÁRÁS

Quarterly Journal of the Hungarian Meteorological Service
Vol. 97, No. 1, January–March 1993

Recent developments in the MAPS isentropic-sigma data assimilation system

S. G. Benjamin, T. L. Smith[1], P. A. Miller, D. Kim[2], T. W. Schlatter, D. Dévényi[3], J.-M. Carrière[4] and R. Bleck[5]

NOAA Environmental Research Laboratories
Forecast Systems Laboratory
Boulder, Colorado 80303, U.S.A.

(Manuscript received 3 September 1992; in final form 22 February 1993)

Abstract—A data assimilation system with a 3-h update frequency has been configured in hybrid isentropic-sigma coordinates. Several changes to this system have either been recently made or are now under development, including a change in the hybrid coordinate structure, addition of model physics, assimilation of satellite radiances, and improved analysis structure functions that allow explicit analysis of the divergent wind component. Short-range forecasts (3-6 hours) from this system are shown to provide improvement over longer-range forecasts (12 hours), indicating that high-frequency asynoptic observations from aircraft and wind profilers can be used successfully to update numerical predictions.

Key-words: data assimilation, isentropic coordinates, mesoscale forecasting, numerical weather prediction.

---

[1] Jointly affiliated with the Cooperative Institute for Research in the Atmosphere, Colorado State University, Ft. Collins, CO

[2] Jointly affiliated with the Cooperative Institute for Research in Environmental Sciences, University of Colorado, Boulder, CO

[3] Permanent affiliation - Hungarian Meteorological Service, Budapest

[4] Permanent affiliation - Météo France, Toulouse

[5] Permanent affiliation - University of Miami, Rosenstiel School of Marine and Atmospheric Science, Miami, Florida

---

Corresponding author address: Dr. S.G. Benjamin, NOAA/ERL/FSL,R/E/FS1, 325 Broadway, Boulder, CO 80303, U.S.A.

1. Introduction

The Mesoscale Analysis and Prediction System (MAPS), a mesoscale data assimilation system now configured in hybrid isentropic-sigma coordinates, has been under development since 1986. MAPS runs in real time at the Forecast Systems Laboratory, currently providing three-dimensional analyses and short-range forecasts over the contiguous United States and adjacent areas every 3 hours. The asynoptic analyses are supported by data from commercial aircraft, wind profilers, and surface reporting stations. Several significant changes have been made to MAPS since the original all-isentropic version was introduced in 1988 (see *Benjamin et al.*, 1991).

2. Hybrid isentropic-sigma coordinates

A hybrid isentropic-sigma ($\theta-\sigma$) coordinate was adopted to provide better resolution of the boundary layer under conditions of neutral static stability while retaining the advantages of θ coordinates in the free atmosphere. Isentropic coordinates give extra resolution in the vicinity of frontal zones and, therefore, better define gradients of temperature, moisture and momentum found in those regions. The initial version of this system, with 18 levels (5 σ levels and 13 θ levels), used a constant-depth σ domain with four layers of 50 hPa each and a fairly smooth surface terrain field. The initial hybrid coordinate configuration is illustrated in *Fig. 1a*, a depiction of analysis/model surfaces on an east-west cross section through the northwestern United States.

A variation of the hybrid coordinate was subsequently developed in which the σ domain is of variable depth, occupying the volume between a detailed surface terrain field and a smoothed $\theta-\sigma$ interface positioned approximately 150 hPa above a smoothed terrain field (*Fig. 1b*). In this variable-depth σ system, the error associated with the σ pressure gradient force is limited to a narrower vertical extent, allowing the use of high-resolution topography. A comparison of topography fields for the 80- and 60-km versions of MAPS is given in *Fig. 2*.

The pressure at the $\theta-\sigma$ interface is specified (time-independent) in the variable-depth σ system. In the original fixed-depth σ system, the interface pressure was time-dependent, a constant pressure thickness above the surface pressure. Tests with calm initial conditions show that this new formulation produces less noise than the hybrid coordinates with a constant-depth σ domain.

At the same time as the change to the variable-depth σ hybrid system, the number of levels was increased from 18 to 25 (6 σ and 19 θ levels). The spacing between isentropes below about 320 K was changed from 6 to 4 K. Also, the horizontal grid spacing was changed from 80 to 60 km. The high-resolution topography for the 60-km MAPS domain is shown in Fig. 2b.

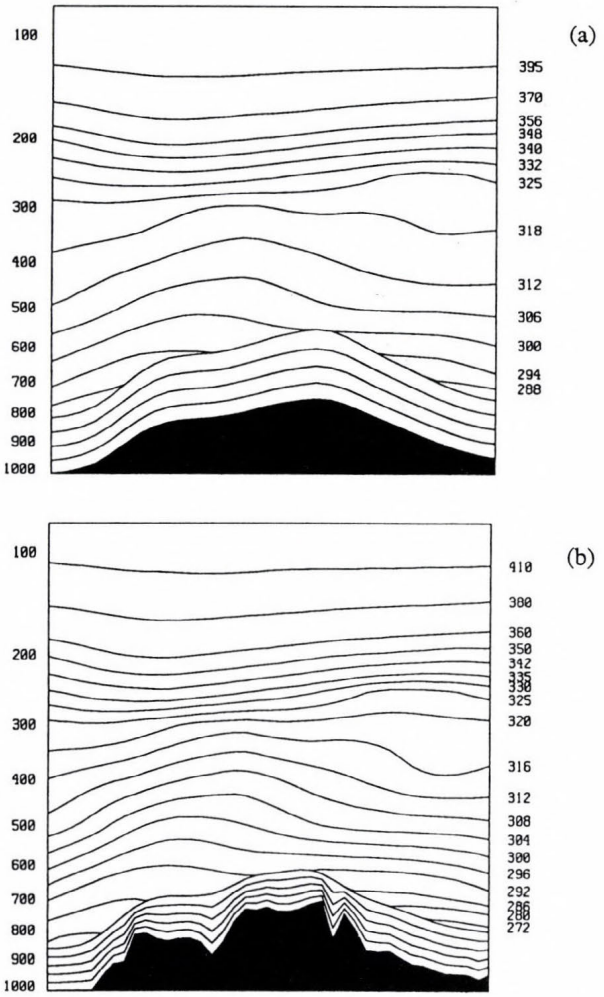

Fig. 1. East-west cross section from the Pacific Ocean off the southern Oregon coast to northern South Dakota for 1200 UTC 1 February 1991. Lines show the positions of MAPS analysis/forecast levels, including isentropic levels (labels on right) and sigma levels parallel to the model terrain. Pressure in hPa is shown on the left. Data are from gridded output of the Nested Grid Model analysis at this time. (*a*) 80-km, 18-level, fixed-σ version of MAPS, (*b*) 60-km, 25-level, variable-σ version of MAPS.

3. Observational data used in MAPS

MAPS incorporates data from several sources available within its current domain: about 80 standard 12-hourly rawinsonde (RAOB) observations, between 600 and 1200 hourly surface airways observations (SAOs), about 25 fixed buoys near the Atlantic and Pacific coastlines, and unconventional data

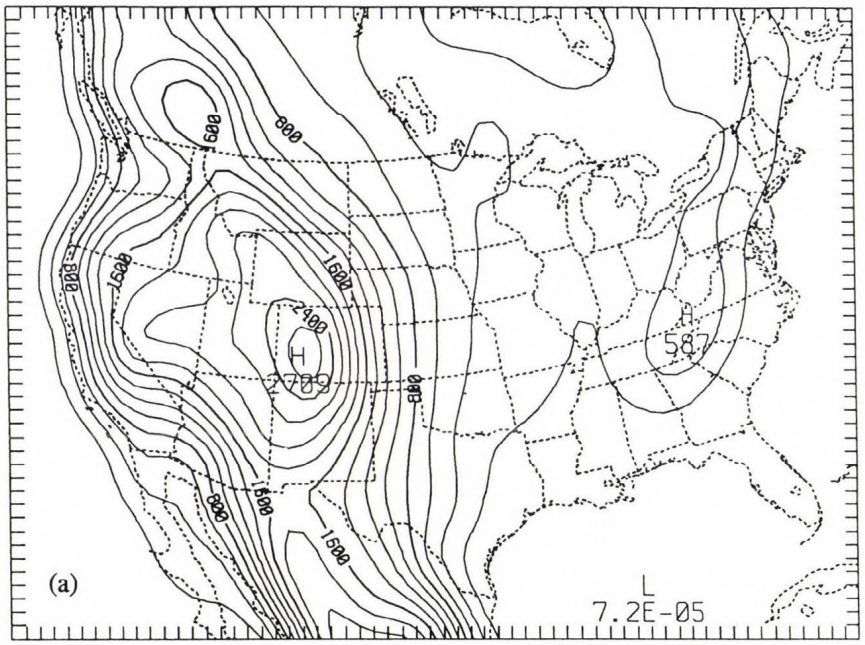

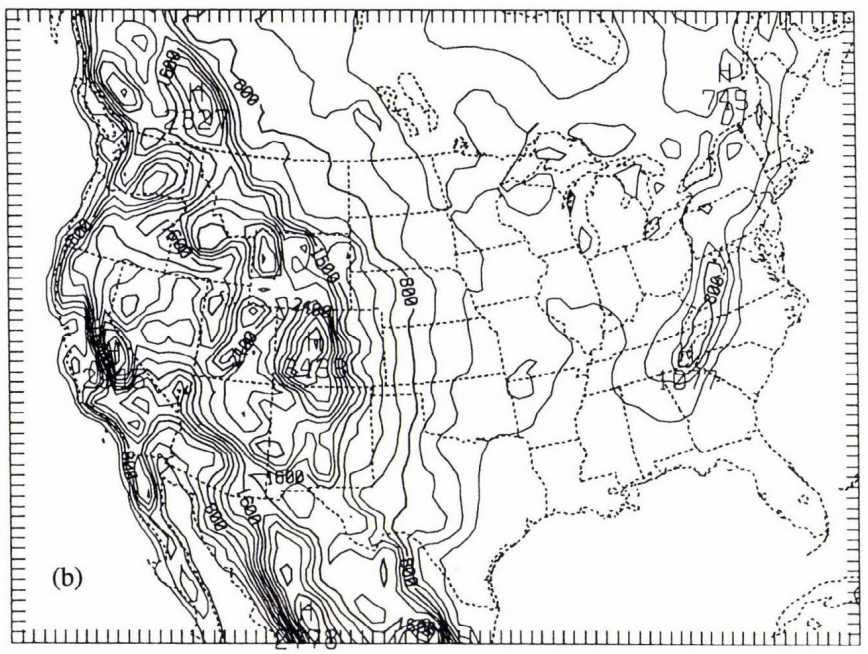

Fig. 2. Comparison of terrain fields for (*a*) 80-km and (*b*) 60-km versions of MAPS.

sources such as wind profilers and automated aircraft reports. With these observations, MAPS produces 3-hourly upper-air analyses.

The wind profiler data come from the NOAA Wind Profiler Demonstration Network, which is concentrated in the central United States (*Chadwick* and *Hassel,* 1987). As of June 1992, about 25 network profilers were operational. The data from all the profilers are 60-min averages of wind by height.

The automated aircraft reports in MAPS arrive via ACARS, the ARINC (Aeronautical Radio, Inc.) Communications, Addressing and Reporting System. Automated wind and temperature reports are typically made every 7.5 minutes by commercial aircraft that are properly equipped. The wind reports are of very high accuracy, owing to the inertial navigation systems onboard the aircraft (*Benjamin et al.,* 1991). Aircraft observations from −2 h to +1 h of the analysis time are used in the analysis. Depending on the time of day, the number of reports used in an analysis ranges from fewer than 400 at 0900 UTC to more than 1500 at 0000 UTC (*Fig. 3*). These reports, now numbering about 8500 per day over the United States, are concentrated in the middle to upper troposphere at standard flight levels.

Lateral boundary conditions for MAPS are specified from forecasts from the National Meteorological Center (NMC) Regional Analysis and Forecast System (RAFS; *Petersen et al.,* 1991). RAFS forecasts are interpolated to MAPS vertical and horizontal coordinates for this purpose.

4. Observational quality control

Incoming data are screened before assimilation into MAPS. The screening takes place in two steps: (1) vertical consistency checks performed on incoming

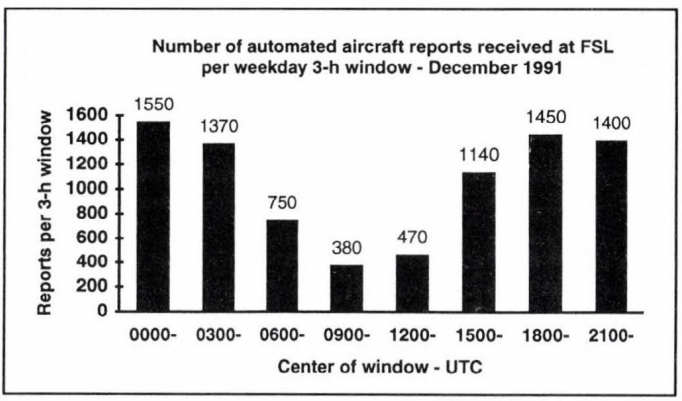

Fig. 3. Number of ACARS reports collected in 3-h intervals throughout the day in December 1991. These numbers were still representative in June 1992.

rawinsonde and wind profiler data and (2) horizontal consistency checks performed on all observations after interpolation to analysis surfaces. These checks are similar to those for the pure isentropic version of MAPS described by *Benjamin et al.* (1991).

Rawinsonde profiles are required to contain reasonable surface data and to be vertically consistent in temperature, height, pressure, and dewpoint. Hydrostatic and lapse-rate checks are employed to check the vertical consistency of heights and temperature. Corrections are made (when possible) based on ideas given in *Gandin* (1988). If correction is not possible, the erroneous levels are flagged as bad and not used in subsequent MAPS quality control, analysis, or forecast components. Wind profiler data are checked for vertical consistency using a gate-to-gate shear threshold, which is a function of height, wind speed, and wind direction. Temporal consistency is also checked by statistically comparing each profiler wind observation to winds from adjacent times and heights (*Brewster* and *Schlatter,* 1989). No corrections are attempted but, as with rawinsonde data, bad levels are flagged and ignored in later processing. After these vertical quality control checks, rawinsonde and profiler data are interpolated to MAPS hybrid coordinate levels.

Each observation is then checked for horizontal consistency by comparing it to surrounding observations at the same level. Surrounding observations are analyzed to the location of the target observation (the observation being checked) using univariate optimal interpolation and MAPS 3-h forecasts as background. If the analyzed residual (difference between observation and background value) minus the observed residual is greater than a threshold, further checking is performed to determine if the target observation or one of the surrounding observations is incorrect. The threshold is a function of analysis error and contains a factor dependent on analysis level and observation type. The factors were updated for the new MAPS domain by studying the statistical properties of the ratio of the threshold to the analysis minus observed values (*Miller* and *Benjamin,* 1991). As before, observations found bad are not used in subsequent processing. Horizontal consistency checks for surface observations are performed separately as part of the MAPS surface assimilation system (*Miller* and *Benjamin*, 1992).

5. Objective analysis in isentropic-sigma hybrid coordinates

Benjamin et al. (1991) described the original MAPS analysis in pure isentropic coordinates. The mass analysis consisted of a two-step procedure, a multivariate mass/wind initial analysis followed by a univariate analysis of mass only. The two-step analysis procedure has been extended in the MAPS hybrid analysis for the mass variable in both the θ and σ domains. Optimal interpolation (OI) is used for multivariate and univariate analyses. Up to 63

observations may influence the analyzed value at a single grid point. Observations are selected as described by *Benjamin* (1989).

In the θ domain, first an *M/u/v* multivariate analysis (where the Montgomery stream function, $M = gz + \Pi\theta$) is performed from which an increment to the Exner function,

$$\Pi = C_p \left(\frac{P}{P_0} \right)^{R/C_p} = \frac{\partial M}{\partial \theta},$$

(with $P_0 = 1000$ hPa) is calculated hydrostatically. This increment is added to the original Exner function background field, forming an updated background field for a subsequent univariate analysis of pressure on θ surfaces.

In the σ domain, a *z/u/v* multivariate analysis is performed at each level. A surface pressure increment is determined from the z increment at the lowest sigma level. A univariate analysis of θ is then performed throughout the σ domain.

One final step is performed for the wind/mass analysis in hybrid coordinates. The original M increment at a reference level in the upper troposphere is saved after the multivariate analysis. Using that updated M value, we hydrostatically integrate back down to the surface and then compare that value of M with M_{sfc} calculated directly from

$$M_{sfc} = gz_{topo} + \Pi_{sfc}\,\theta_{sfc}.$$

A temperature adjustment is then calculated and applied to the column between the surface and the reference θ level. In this manner, the original multivariate M increment at the reference level is assured even after hydrostatic integration. The reference level, chosen to be in the upper troposphere, is considered to be most reliable because it is close to the layer of dense aircraft report coverage.

The moisture variable used in MAPS is condensation pressure (P_c), which is the lifting condensation level for a given parcel of air. P_c is conserved for motion on isentropic surfaces if no condensation or evaporation occurs, and it varies much more linearly through the troposphere than water vapor mixing ratio. A univariate OI analysis of P_c is performed in which the P_c increments are streaked elliptically along the wind in a manner similar to that described by *Benjamin* and *Seaman* (1985).

Previously, the coefficients for models describing horizontal correlation of background error used in MAPS were based on statistics of 12-h errors collected by *Benjamin* (1989) from the Nested Grid Model (NGM) run at NMC. Recently, *Carrière* (1991) collected new statistics on 3-h forecast errors from the MAPS prediction model. As of March 1991, new coefficients for the

second-order autocorrelation model (SOAR) of horizontal correlation of forecast error had been implemented based on Carrière's study.

Analyses on isentropic levels may use observations both above and below the $\theta-\sigma$ interface; the position of the interface is not relevant. The σ and θ level analyses are redundant in a sense, since the domains usually overlap, and analyses are performed on both sets of surfaces separately. This is done to ensure the best possible θ analyses just above the interface by using data on both sides of the interface. Before a hybrid analysis is used to initialize the hybrid forecast model, however, information on θ levels beneath the interface is truncated and isentropic levels beneath the interface are forced to become collocated with the interface, as shown in Figs. 1 and 2.

Observation selection is done on θ surfaces in the θ domain and on σ surfaces in the σ domain. The three-dimensional correlations of forecast error are partitioned into horizontal and vertical components in both σ and θ domains, where the vertical component is based on potential temperature separation. The use of this "vertical" correlation model in the σ domain can result in sharp horizontal gradients along σ surfaces that are consistent with observed air-mass discontinuities.

6. Experiments with assimilating satellite radiances into MAPS analyses

Satellite data have not been utilized by MAPS yet in real time, but testing in this area has been conducted for the last few years. Because of complications in the temperature retrievals of satellite radiance data, a radiance assimilation scheme has been designed for MAPS based on the scheme of *Eyre* and *Lorenc* (1989). At each field of view of the Television and Infrared Observation Satellite (TIROS) pass within the MAPS analysis domain, a temperature/humidity profile from the 3-h MAPS forecast is interpolated from hybrid to pressure coordinates in order to compute radiances. Satellite radiance residuals (difference between measured and computed radiances) are calculated, from which an analysis increment field can be obtained using an off-line empirical retrieval operator.

The retrieval operator that converts radiance residuals to the temperature or humidity increment is a covariance matrix obtained from the collocated data set of (1) measured radiances, (2) computed radiances from 3-h MAPS forecast, (3) computed radiances from RAOB, (4) RAOB profiles and (5) 3-h MAPS forecast profiles. The retrieval operator is further refined by obtaining covariance matrices from smaller (in the sample size) but more homogeneous (in the distribution of errors) collocated data sets. This is achieved by classifying the data set into several clusters according to closeness in the data. Each cluster represents different covariances because of different error characteristics in the forecast field. A preliminary study of cluster analyses with a March 1991 data set was reported by *Kim* (1992).

7. Development of new structure functions for MAPS objective analyses

The MAPS wind field analysis is currently based on the geostrophic relationship using a geostrophic coupling coefficient to allow some ageostrophy. Because divergence plays an important role in mesoscale processes, use of the geostrophic approximation in a mesoscale model is questionable. Applying the kinematic theory of homogenous and isotropic turbulence, *Daley* (1985) developed a new approach to determine background error correlation functions for mass and wind forecasts that includes an explicit analysis of the divergent wind component. The European Centre for Medium-Range Weather Forecasts (ECMWF) has followed Daley's formulation in modeling wind and mass field first guess errors (*Hollingsworth* and *Lönnberg*, 1986; *Lönnberg* and *Hollingsworth*, 1986). A similar formulation is under development at MAPS for implementation in a 3-h data assimilation cycle.

Based on the Helmholtz theorem, a long but straightforward derivation (*Daley*, 1991, pp.155-169; *Schlatter* and *Carrière*, 1991) results in the following system of equations for autocorrelation and cross-correlation functions (ρ) of Montgomery stream function (M), velocity potential (χ), and stream function (ψ):

$$-\frac{1}{D^2}\left(\frac{d^2}{dx^2}+\frac{1}{x}\frac{d}{dx}\right)\left[\gamma^2\,\rho_{\psi\psi}(x)+\delta^2\,\rho_{\chi\chi}(x)\right]=\rho_{ll}(x)+\rho_{tt}(x) \tag{1}$$

$$\frac{1}{D^2}\left(\frac{d^2}{dx^2}-\frac{1}{x}\frac{d}{dx}\right)\left[\gamma^2\,\rho_{\psi\psi}(x)-\delta^2\,\rho_{\chi\chi}(x)\right]=\rho_{ll}(x)-\rho_{tt}(x) \tag{2}$$

$$-\frac{\gamma\,\delta}{D^2}\left(\frac{d^2}{dx^2}-\frac{1}{x}\frac{d}{dx}\right)\rho_{\psi\chi}(x)=\rho_{lt}(x)=\rho_{tl}(x) \tag{3}$$

$$\frac{\gamma}{D}\frac{d}{dx}\rho_{M\psi}(x)=\rho_{Mt}(x) \tag{4}$$

$$\frac{\delta}{D}\frac{d}{dx}\rho_{M\chi}(x)=\rho_{Ml}(x) \tag{5}$$

$$\rho_{MM}(x)=\rho_{MM}(x). \tag{6}$$

In the system of Eqs. (1)−(6), D signifies a distance beyond which correlations are expected to be a small constant value, giving a natural scaling for separation distance ($x=r/D$). In our investigation, a value for D of 3000 km was used. Standard deviations of background error for the stream function and velocity potential have been normalized by the standard deviation of background error for the transverse (t) wind component (or equivalently, because of isotropy, by the standard deviation of background error for the longitudinal (l) wind component), resulting in $\gamma=\sigma_\psi/\sigma_l$ and $\delta=\sigma_\chi/\sigma_l$. (The t and l wind components are defined as the wind components normal and parallel, respectively, to the line segment connecting the pair of points, as shown by *Daley* (1991, p.158).) Eq. (6) is added to the system for completeness. The background error correlations on the right-hand sides of Eqs. (1)−(6) are considered to be known. They may be computed from a sample of forecasts by the assimilating model.

The system of equations above can be solved if the unknown correlations on the left are represented by a truncated expansion of Bessel functions.

$$\rho_{unknown}(x) = \sum_{i=1}^{N} y_i^{unknown} J_0(k_i x). \tag{7}$$

The unknown coefficients y_i are to be determined, and J_0 is a Bessel function of the first kind of order zero. The coefficients k_i are the positive roots of $J_1(k)=0$, corresponding to a zero, Neumann-type boundary condition at D. Substituting expressions like (7) into the left-hand side of Eqs. (1)−(6) and the empirical correlation values into the right-hand sides yields a fully determined system for the unknown coefficients of the truncated Bessel function series. Because of unavoidable noise in the empirical correlations, it is preferable to use a least squares technique to solve for the coefficients.

To achieve this solution, knowledge of the parameters γ and δ is required. But in the case of a limited area model such as MAPS, stream function and velocity potential fields cannot be computed uniquely because they depend on actual lateral boundary conditions. Therefore the following method for iterative estimation of these parameters has been developed. In addition to the system of Eqs. (1)−(6), a diagnostic relationship can be obtained from turbulent microscale theory. To do this, a two-dimensional length scale L has been defined for any autocorrelation function ρ as

$$L^2 \equiv -2\left[\frac{\rho(r/D)}{\nabla^2 \rho(r/D)}\right]_{r\to 0}, \tag{8}$$

where, for the isotropic case,

$$\nabla^2 = \left(\frac{d^2}{dr^2} + \frac{1}{r} \frac{d}{dr} \right).$$

Using (8), (7), and (1), one can derive the following relationship between stream-function length scale L_ψ and velocity potential length scale L_χ (*Daley*, 1991, p.160):

$$\frac{\gamma^2}{L_\psi^2} + \frac{\delta^2}{L_\chi^2} = 1, \tag{9}$$

where

$$L_\psi^2 = \frac{2D^2}{\sum_{i=1}^{N} k_i^2 \psi_i}, \qquad L_\chi^2 = \frac{2D^2}{\sum_{i=1}^{N} k_i^2 \chi_i}. \tag{10}$$

The ratio $\nu^2 = \delta^2 / L_\chi^2$ in (9) is equivalent to the kinetic energy in the divergent component of the forecast error normalized by total forecast error kinetic energy.

Using (7), (9), and (10), an iterative least squares method can be developed such that the solution of (1) and (2) is represented by a convergent series of unknown coefficients ψ_i and χ_i. The value of ν is iterated until the distance between the empirical and modeled correlations is minimized.

To illustrate the results of the above procedure, *Fig. 4* shows the autocorrelation of 3-h MAPS forecast error for the Montgomery stream function on the 312 K isentropic level. Note that the sample size for all but the smallest separation distance is 3000. The correlation approaches slowly a small negative value, suggesting a slight large-scale bias in the Montgomery field. Considering the correlations ρ_{ll} and ρ_{tt} we find, similar to *Hollingsworth* and *Lönnberg* (1986), that the longitudinal correlation falls off less rapidly with distance than the transverse correlation. It does not approach zero until beyond 1000 km whereas the transverse correlation becomes negative around 500 km. Corresponding solutions of Eqs. (1) and (2) show that the original behavior of empirical correlations has been retained, but the results are corrected by zero intercept values containing the effects of measuring errors and unresolved scales in the MAPS model. The correlations ρ_{Mt} and ρ_{Ml} are illustrated in *Figs. 5a* and *5b*. The value of ρ_{Mt} reaches a minimum at $r=400$ km and then returns to near zero throughout the rest of its range. The fact that our ρ_{Mt} dips beyond 1000 km only to -0.25 suggests that our 3-h background errors are relatively less geostrophic than those at ECMWF (compare with Fig. 16 of *Lönnberg* and *Hollingsworth* (1986), where the $Z-t$ correlation dips to -0.55). Note that ρ_{Ml} is near zero throughout its range. *Fig. 6* (fitted $\rho_{M\psi}$) gives another illustration of

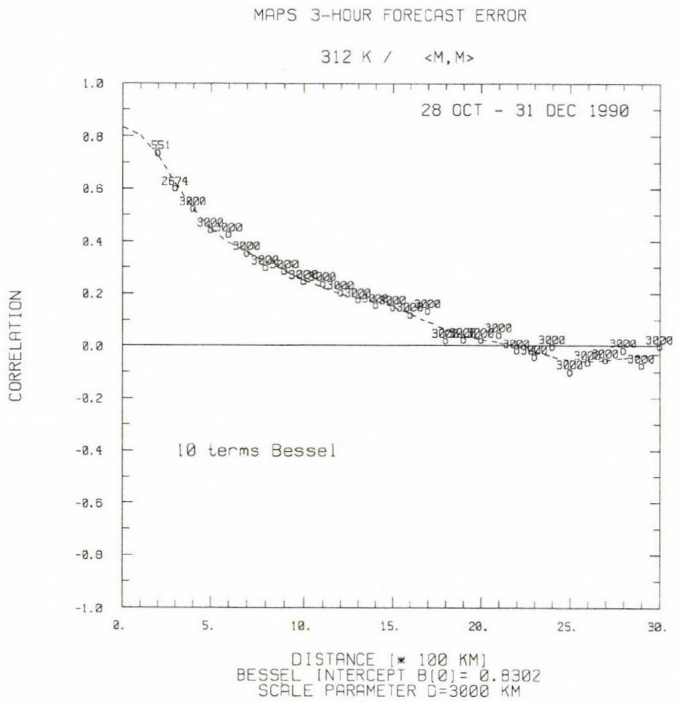

Fig. 4. Correlation of Montgomery stream function on the 312 K isentropic level. The open circles are empirical correlation values computed from 3-h MAPS forecast errors during the winter of 1990 and 1991. The dashed line depicts the fitted Bessel function expansion.

the ageostrophic character of MAPS forecast errors. If the 3-h forecast errors of the MAPS model were purely geostrophic, one would expect $\rho_{M\psi}$ to approach one at zero separation. Instead, it reaches 0.39 for the winter data, indicating substantial ageostrophy in the error field.

The statistics described above for the 312 K isentropic level have also been computed for another 12 θ and 5 σ levels in the MAPS model. Since calculating 10-term Bessel expansions for every correlation in the analysis program would be very expensive, we plan to precompute them at 1-km resolution. From these look-up tables, the correlations actually used in the analysis are easily computed.

This method for determining new forecast error structure functions and preliminary results from it are the first steps in the modernization of the MAPS objective analysis system. Determination of the vertical correlation structure for M, ψ, and χ background error fields is not yet complete. Applying new corre-

Fig. 5. Cross-correlations between the Montgomery stream function and the longitudinal and transverse wind components 3-h MAPS forecast errors on the 312 K isentropic level. Legends are as in Fig. 4. (*a*) ρ_{Mt} correlations, (*b*) ρ_{Ml} correlations.

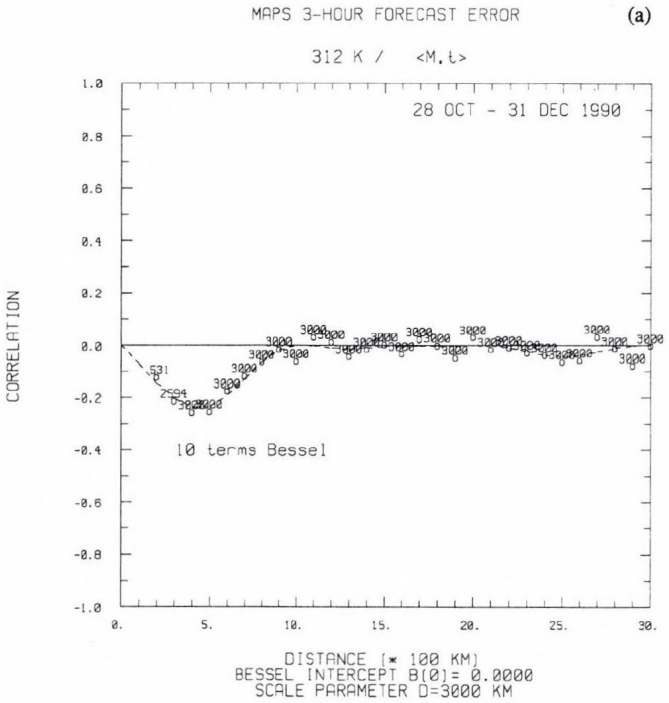
MAPS 3-HOUR FORECAST ERROR
(a)
312 K / <M,t>
28 OCT - 31 DEC 1990
CORRELATION
1.0
0.8
0.6
0.4
0.2
0.0
-0.2
-0.4
-0.6
-0.8
-1.0
0.
5.
10.
15.
20.
25.
30.
10 terms Bessel
DISTANCE (* 100 KM)
BESSEL INTERCEPT B(0)= 0.0000
SCALE PARAMETER D=3000 KM

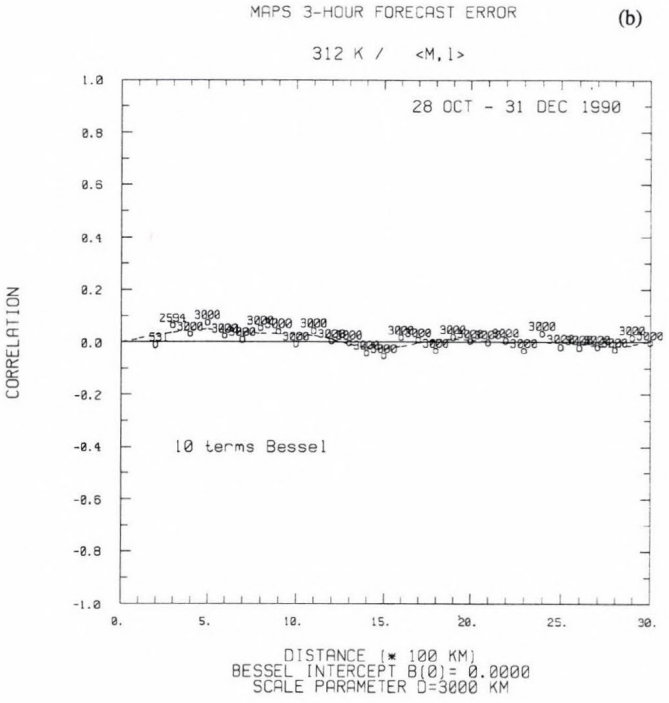
MAPS 3-HOUR FORECAST ERROR
(b)
312 K / <M,l>
28 OCT - 31 DEC 1990
CORRELATION
1.0
0.8
0.6
0.4
0.2
0.0
-0.2
-0.4
-0.6
-0.8
-1.0
0.
5.
10.
15.
20.
25.
30.
10 terms Bessel
DISTANCE (* 100 KM)
BESSEL INTERCEPT B(0)= 0.0000
SCALE PARAMETER D=3000 KM

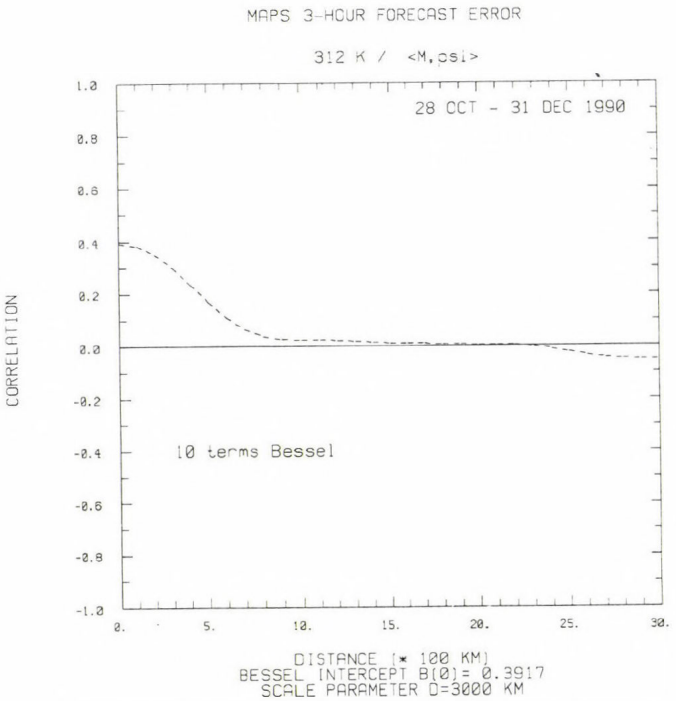

Fig. 6. $\rho_{M\psi}$ correlations on the 312 K isentrope by solution of Eq. (4). The dashed line depicts the fitted Bessel function expansion.

lation functions for dynamical variables of the MAPS objective analysis could also lead to an improved method for the humidity analysis, including application of total precipitable water information derived from GOES satellite data.

8. *Isentropic-sigma hybrid forecast model*

The forecast model used in MAPS is a descendant of the primitive equation model developed by *Bleck* (1974, 1977, 1984). The MAPS version of the Bleck model uses non-staggered vertical levels to avoid vertical interpolation between analyses and forecasts in the MAPS assimilation cycle.

The primary recent numerical innovation in the MAPS model has been the incorporation of the hybrid coordinate system. The prognostic variables are pressure thickness, P_c, and u/v wind components in the θ domain, and potential temperature, P_c, u, and v in the σ domain. Following Fig. 1, isentropic coordinate surfaces are allowed to intersect the $\sigma-\theta$ interface because θ is variable along the interface. Computationally, the interface plays a role similar to that of the ground in pure isentropic models. Isentropic layers collapse to a state of zero layer thickness on the interface.

Since the interface is not a material surface, the σ and θ domains are permitted to exchange mass (and other properties). The vertical component of motion across the interface is determined through integration of the continuity equation. The pressure thickness in isentropic layers above the interface is adjusted so that entropy and mass in the column are conserved.

Precipitation physics has also been added to the MAPS model. Stable precipitation is determined by excess moisture over saturation—saturation occurring when the condensation pressure equals the pressure at a grid point. There is currently no evaporation of stable precipitation in layers below the supersaturated level. Convective precipitation is estimated via the parameterization developed by *Grell* (1992); the effects of evaporation and convective downdrafts are included. The closure assumption in the Grell scheme is the rate of destabilization.

A scheme for vertical turbulent mixing based on the level-2.0 turbulence closure of *Mellor* and *Yamada* (1982) has also been added to MAPS. The scheme acts primarily in the boundary layer, but can also mix layers aloft with sufficiently low Richardson numbers. Even without realistic surface fluxes, the Mellor-Yamada second-order scheme produces much improved profiles of potential temperature and wind near the surface. Work is under way to add a surface energy budget and surface flux formulations to the MAPS model, including effects of cloudiness on downward shortwave and longwave fluxes.

9. Statistical verification

Statistical verification of MAPS forecasts against rawinsonde data has shown a steady improvement over the last 30 months as modeling and analysis improvements have been implemented. The changes most responsible for statistical improvement include elimination of errors in data ingest, analysis, and forecast model routines as well as planned improvements. These improvements include the implementation of the hybrid coordinate system in May 1990, the Grell convective scheme in September 1990, and the 60-km/25-level variable-σ system with the Mellor-Yamada mixing in September 1991. The volume of observations has not changed appreciably during this period.

The use of isentropic coordinates and extra aircraft observations in MAPS allows improved short-range forecasts of jet-level winds. This is evident in the recent history of verification of 250-hPa wind forecasts (*Fig. 7*). MAPS 3-h forecasts, using asynoptic observations, currently improve on NGM 12-h forecasts (not using asynoptic data) by well over 1 m s^{-1}. This margin of improvement over NGM forecasts has increased substantially during the comparison period. Six-hour forecasts from MAPS have also generally shown improvement over 12-h NGM forecasts in the upper troposphere since they started running in January 1991. The distribution of wind forecast errors with

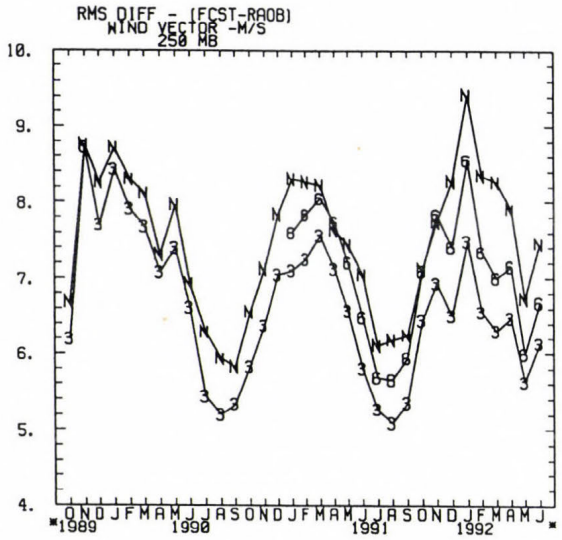

Fig. 7. RMS vector difference between forecasts and rawinsonde observations of 250-hPa winds from October 1989 to June 1992. NGM 12-h forecasts are denoted as **N**, 3-h MAPS forecasts as **3**, and 6-h MAPS forecasts as **6**.

height is shown in *Fig. 8a* for early 1992. The greatest advantage of frequent assimilation is in the high troposphere, where ACARS reports are most plentiful.

Height forecasts from MAPS with durations of 3 hours and even 6 hours currently show improvement of 1−2 m (standard deviation error) over 12-h NGM height forecasts at all mandatory levels up to 150 hPa (*Fig. 8b*). The difference is most pronounced near jet level and near the surface. During the winter of 1990-91 when the pure isentropic version of MAPS was running, 3-h MAPS forecasts were poorer than 12-h NGM forecasts of height at all mandatory levels (*Benjamin et al.*, 1991). This indicates the progress that has occurred since that time. Data sensitivity experiments done by *Benjamin* and *Stamus* (1991) show that surface observations are quite helpful in improving low-level height forecasts, and also have some positive impact in height forecasts throughout the troposphere.

10. Plans for the future

The current MAPS assimilation cycle produces upper-level analyses and forecasts every 3 hours. *Benjamin* and *Stamus* (1991) have shown that there are already sufficient asynoptic data over the United States to run an assimilation cycle at 1-h frequency with the potential for modest improvements over a 3-h cycle. Their tests were run with a case from January 1990, when wind profiler

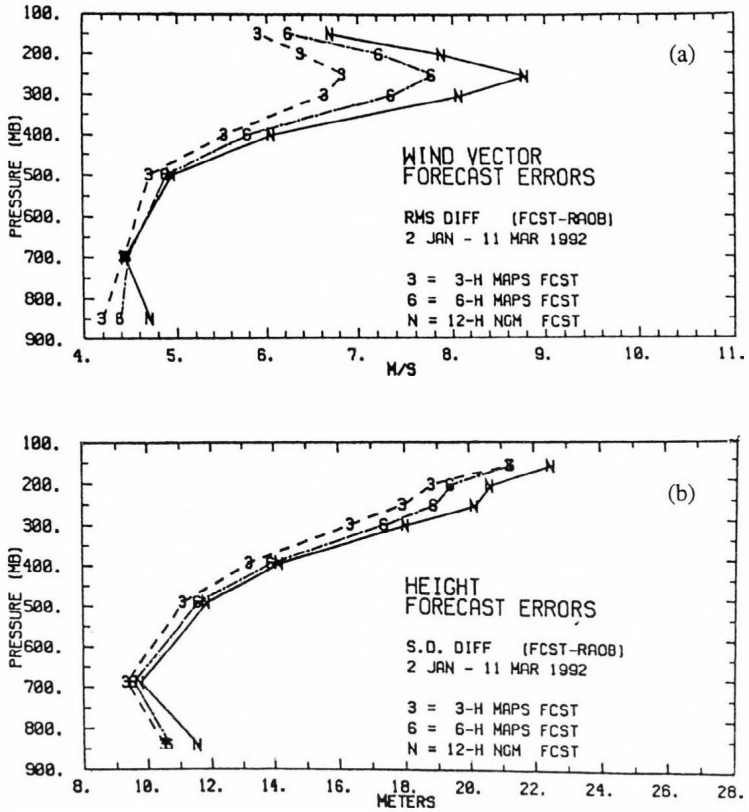

Fig. 8. Vertical profiles of forecast errors (difference from rawinsonde observations at forecast verifying time) for the period 2 January–11 March 1992. Symbols are as in Fig. 7. (*a*) Root-mean-square vector error of wind forecasts, (*b*) standard deviation error of height forecasts.

data were available only from a few experimental sites in Colorado. As the number of wind profilers producing hourly data increases, the potential improvement from a 1-h cycle will also increase.

Improvements in handling diurnal surface effects have been implemented during the remainder of 1992. In 1993, the MAPS analysis in hybrid vertical coordinates will be recast to allow explicit analysis of the divergent wind component (*Schlatter* and *Carrière,* 1991).

After real-time testing at the Forecast Systems Laboratory, these improvements will be incorporated into a version of MAPS now running experimentally at NMC. MAPS is expected to run regularly at NMC beginning in 1993.

Acknowledgments—The authors acknowledge the contributions of *Kevin Brundage* and *Pan Zaitao* in the development of MAPS. *Chris Thomas* and *Pete Stamus* gave careful reviews of the paper.

D. Dévényi's work was supported by a National Research Council (NRC) - NOAA/ERL/Forecast Systems Laboratory Research Associateship. He would like to thank the MAPS team for assistance during his visit.

References

Benjamin, S.G., 1989: An isentropic meso-alpha scale analysis system and its sensitivity to aircraft and surface observations. *Mon. Wea. Rev. 117*, 1586-1605.

Benjamin, S.G. and *Seaman, N.L.*, 1985: A simple scheme for objective analysis in curved flow. *Mon. Wea. Rev. 113*, 1184-1198.

Benjamin, S.G. and *Stamus P.A.*, 1991: Experiments with 1-h and 3-h assimilation cycles using mesoscale aircraft and surface data. *Preprints, 9th Conference on Numerical Weather Prediction*, Denver, Colorado, 14-18 October. American Meteorological Society, Boston, Massachusetts, 186-189.

Benjamin, S.G., Brewster, K.A., Brümmer, R.L., Jewett, B.F., Schlatter, T.W., Smith, T.L. and *Stamus, P.A.*, 1991: An isentropic three-hourly data assimilation system using ACARS aircraft observations. *Mon. Wea. Rev. 119*, 888-906.

Bleck, R., 1974: Short range prediction in isentropic coordinates with filtered and unfiltered numerical models. *Mon. Wea. Rev. 102*, 813-829.

Bleck, R., 1977: Numerical simulation of lee cyclogenesis in the Gulf of Genoa. *Mon. Wea. Rev. 105*, 428-445.

Bleck, R., 1984: An isentropic coordinate model suitable for lee cyclogenesis simulation. *Riv. Meteor. Aeronaut. 44*, 189-194.

Brewster, K.A. and *Schlatter, T.W.*, 1989: Recent progress in automated quality control of wind profiler data. *Preprints, 8th Conference on Numerical Weather Prediction*, Baltimore, Maryland. American Meteorological Society, Boston, Massachusetts, 331-338.

Carrière, J.-M., 1991: Statistics of horizontal correlation of errors for three-hour prediction fields in isentropic coordinates. *Preprints, 9th Conference on Numerical Weather Prediction*, Denver, Colorado, 14-18 October. American Meteorological Society, Boston, Massachusetts, 62-65.

Chadwick, R.B. and *Hassel, N.*, 1987: Profiler: the next generation surface-based atmospheric sounding system. *Preprints, Third International Conference on Interactive Information and Processing Systems for Meteorology, Oceanography and Hydrology*, 12-16 January, New Orleans, Louisiana. American Meteorological Society, Boston, Massachusetts, 15-21.

Daley, R., 1985: The analysis of synoptic scale divergence by a statistical interpolation procedure. *Mon. Wea. Rev. 113*, 1066-1079.

Daley, R., 1991: *Atmospheric Data Analysis*. Cambridge University Press, New York.

Eyre, J.R. and *Lorenc, A.C.*, 1989: Direct use of satellite sounding radiances in numerical weather prediction. *Meteor. Mag. 118*, 13-16.

Gandin, L.S., 1988: Complex quality control of meteorological observations. *Mon. Wea. Rev. 116*, 1137-1156.

Grell, G., 1992: Prognostic evaluation used by cumulus parameterization schemes. *Mon. Wea. Rev. 120*, in press.

Hollingsworth, A. and *Lönnberg, P.*, 1986: The statistical structure of short-range forecast errors as determined from radiosonde data. Part I: The wind field. *Tellus 38A*, 111-136.

Kim, D., 1992: Cluster analyses of radiance data measured from satellite and computed from forecast profiles. *Preprints, Twelfth Conference on Probability and Statistics in the Atmospheric Sciences*, 22-26 June, Toronto, Canada. American Meteorological Society, Boston, Massachusetts, J109-112.

Lönnberg, P. and *Hollingsworth, A.*, 1986: The statistical structure of short-range forecast errors as determined from radiosonde data. Part II: The covariance of height and wind errors. *Tellus 38A*, 137-161.

Mellor, G.L. and *Yamada, T.*, 1982: Development of a turbulence closure model for geophysical fluid problems. *Rev. Geophys. Space Phys. 20*, 851-875.

Miller, P.A., and *Benjamin, S.G.*, 1991: Horizontal quality control for a real-time 3-h assimilation system configured in isentropic coordinates. *Preprints, 9th Conference on Numerical Weather Prediction*, Denver, Colorado, 14-18 October. American Meteorological Society, Boston, Massachusetts, 58-61.

Miller, P.A. and *Benjamin, S.G.*, 1992: A system for the hourly assimilation of surface observations in mountainous and flat terrain. *Mon. Wea. Rev. 120*, 2342-2359.

Petersen, R.A., DiMego, G.J., Hoke, J.E., Mitchell, K.E., Gerrity, J.P., Wobus, R.L., Juang, H. and *Pecnick, M.J.*, 1991: Changes to NMC's Regional Analysis and Forecast System. *Weather and Forecasting 6*, 133-141.

Schlatter, T.W. and *Carrière, J.-M.*, 1991: A correlation model allowing for divergent wind analyses and supporting three-hour assimilation of mesoscale data. *Preprints, 9th Conference on Numerical Weather Prediction*, Denver, Colorado, 14-18 October. American Meteorological Society, Boston, Massachusetts, 58-61.

IDŐJÁRÁS

Quarterly Journal of the Hungarian Meteorological Service
Vol. 97, No. 1, January–March 1993

Effects of the large-scale circulation on local climate anomalies in relation to GCM outputs

J. Mika

Hungarian Meteorological Service, H-1525 Budapest P.O.Box 38, Hungary

(Manuscript received 2 November 1992; in final form 1 April 1993)

Abstract—A possible way to apply General Circulation Models (GCMs) in regional climate scenarios is to consider the changes in the frequency distribution of model-generated macrocirculation types, and combine them with conditional climatology of each macrotype calculated from the present climate. This can be successful, if a great part of local climate anomalies is connected to frequency anomalies of the macrotypes. To test this assumption, a diagnostic method for separation of circulation and non-circulation factors in local climate anomalies is developed (also allowing a mixed term), based on the classification of *Ambrózy et al.* (1983, 1984), which is an objective modification of that introduced by *Hess* and *Brezowsky* (1969). Results of separation for monthly temperature and precipitation anomalies for Kecskemét, Hungary (47°N 20°E) are presented, for which a secondary role of the circulation factor is experienced, except for the low precipitation anomalies. The annual course in the weight of this term (maximum in winter) is considerable, except for the high precipitation groups. Extracting more information from series of macrosynoptic types than just their monthly frequencies is recommended.

Key-words: GCM-outputs, regional climate scenarios, Hungary, macrocirculation types, temperature, precipitation.

1. Introduction

Estimation of regional features of the expected global warming is one of the actual problems in the greenhouse-gas issue. The use of General Circulation Models (coupled with ocean models, as a tendency, allowing time-dependent simulations of gradual changes) is practically the only way to get information about regional features of global changes, assumed to be larger than that covered by direct instrumental observations.

However, the spatial resolution of GCMs is constrained for practical reasons

by the speed and memory of computers. An increase in resolution not only increases the memory needs, but also leads to a reduction in the required time step. Therefore, in spite of earlier trials (e.g. *Kim et al.*, 1984), the coarsely resolved GCM-outputs cannot be directly used for this goal, while the inadequacy of pure geometrical interpolation (e.g. *Cohen* and *Allsopp,* 1988) has recently been discussed by *Grotch* and *MacCracken* (1991). It is also not a real help from the impact point of view, if climate consequences are expressed in averages for larger areas, e.g. spherical rectangles, of tens of geographical degrees wide, as defined by *Mitchell et al.* (1990). Due to the scaling problem, a visual interpolation from output maps (*Mika,* 1991), losing some information, but also smoothing the grid-specific errors of the field, might be an alternative among the one-step trials in applying GCM-outputs for regional scenarios.

More sophisticated efforts to use GCM-outputs for regional climate scenario construction can be sorted into two groups. In both approaches, however, accuracy of the large-scale flow generated in the GCM is crucial.

The first possibility is a *one way-coupling* of a limited-area model into the original sequence of GCM-fields. From this approach, which is not closely related to the subject of this paper, one can learn at least (*Giorgi et al.,* 1990) that regional climatic patterns, both of the present state and of greenhouse-gas disturbed ones, fail to be well simulated on the coarse grid, comparing to the finer one. Simulations in the latter, however, agree well with high-resolution observations and show considerable geographical details, that cannot be portrayed in original GCMs.

The second way is *to combine* larger scale averages, or main components of the *model-generated fields with empirical relationships*, learned on measured data sets between the large scale characteristics and the regional-scale climate elements. This approach has opened new perspectives for empirical analysis of synchronous processes. Limitation of the statistical approach is, however, that it can only be applied with success, if strong connections between the large-scale parameters and regional climate anomalies exist.

Not referring to earlier works on synchronous connections, generally motivated by long-range forecasting needs (e.g. *Klein* and *Yang,* 1986), there are three often quoted recent studies, representing different approaches in their details.

Karl et al. (1990) used free-atmosphere parameters in the closely located grid-points for independent variables in the belief that their fields were less sensitive to the sub-grid scale details, scarcely simulated in the GCMs. *Wigley et al.* (1990) used areal averages around the locality of interest (Oregon, USA) for the elements (temperature, precipitation) intended to estimate from outputs of a GCM. It was found, that for some locations the majority of local variance could be attributed to large scale effects, but there were wide areal variations in the extent, to which the larger scale anomalies were the determining factors.

In both approaches, a relationship between local anomalies and larger scales containing this locality are established. The third way is based on pressure fields from a wider area, containing also distant localities. *Von Storch et al.* (1991) used canonical correlation analysis relating the rainfall field over the Iberian Peninsula to the observed sea-level pressure field of the Atlantic Sector, in winter. This technique successfully reproduced the observed rainfall patterns, but only the half of the interannual variability was explained. Though the global-scale pressure pattern was fairly well simulated by the applied GCM, the model itself reproduced the precipitation fields with large deficiencies, probably due to the imperfectly treated physics of rainfall. Similar technique for the same GCM was applied by *Werner* (1992) for Central European temperatures in winter. Large part of anomalies was controlled by patterns of Northern Atlantic pressure field, however, on time scales of several decades the trends were controlled by other processes, too.

Pressure information can be related to local climate also in a different way (*Bogardi et al.*, 1992, *Matyasovszky et al.*, 1992). In these works the sequence of previously determined macrosynoptic types is coupled to the series of local weather (precipitation, or indices derived from it) through the probability distribution of conditional Markovian processes. This approach was illustrated by winter precipitation and summer drought indices, but it still has to be verified on broader set of model-generated fields and climate elements. This theoretically sophisticated method, however, requires long series of daily weather elements in order to provide well-defined probability distributions, as free from sample errors as possible.

Our *present paper*, therefore, is dedicated to a less complicated use of macrocirculation types for GCM-related regional climate scenarios. It is suggested to use just the anomalies in the frequencies for all macrotypes, assuming that they produce conditional distributions, being not so well-defined, but easier to realize in practice.

To test this approach, a method is introduced to calculate the relative weight of anomalies in the frequency of macrocirculation patterns relative to time averaged climate anomalies. After describing this method (*Section 2.1*), the applied objective macrosynoptic classification (*Section 2.2*) and the data sets used for the test (*Section 2.3*) is presented. Results for temperature (*Section 3.1*) and pressure (*Section 3.2*) are discussed in *Section 4* in relation with the suggested approach.

2. Methods and data

2.1 The method of separation

The aim of this method is to quantify, what part of climate anomalies can

be directly attributed to the anomalous frequency distribution of macrosynoptic types in the period for which the anomaly is formed. The following elementary operations will conclude at a separation of the anomalies, where this term is one of their three, non-zero components.

Let us have a macrosynoptic classification, containing M disjunct macrotypes. Assuming that the i-th day of the record is characterized by the I-th macrotype, the value of an appropriate weather element can be characterized as $A_I(i)$. The difference between this actual value and its climatological mean is $\Delta A_I(i)$, where

$$\Delta A_I(i) = A_I(i) - \{A\}. \tag{1}$$

Let us further introduce the conditional climatic average $\{A_I\}$ related to the I-th macrotype in the same period as for the unconditional $\{A\}$. Let us add to, and subtract from Eq. (1) $\{A_I\}$. Then $\Delta A_I(i)$ can be divided into two parts:

$$\Delta A_I(i) = [A_I(i) - \{A_I\}] + [\{A_I\} - \{A\}] = A_I'(i) + \{\Delta A_I\}, \tag{2}$$

where $A'_I(i)$ is the actual anomaly relative to the conditional climate average; $\{\Delta A_I\}$ is the difference between conditional and unconditional climate averages.

So the second term is the part of daily weather anomalies which is fully determined by the macrotype itself. The first term, however, is the part of anomalies which can not be estimated at all, if knowing just the actual macrotype.

Let us further have a period which is much shorter than that used for climate averages. For this period, the mean anomaly related to macrotype I is designated by $<\Delta A_I>$. Omitting (i) indices from Eq. (2), this term is averaged as

$$<\Delta A_I> = <A_I'> + \{\Delta A_I\}. \tag{3}$$

(Here and in the next formula, symbols of shorter averaging are not marked in connection with the longer-term averages.)

Within the shorter period for which components of the anomalies are being investigated, the actual relative frequency of the I-th macrotype, $<q_I>$ can also be divided into its climatological relative frequency $\{q_I\}$ and anomaly $<q'_I>$, similarly to the way followed in Eqs. (2) and (3):

$$<q_I> = \{q_I\} + <q_I'>. \tag{4}$$

Approaching to our goal, the anomaly of the whole period, $<\Delta A>$ is equal to

the sum of average conditional anomalies, weighted by relative frequencies of the specific macrotypes:

$$< \Delta A > = \sum_{I=1}^{M} < q_I > < \Delta A_I > . \tag{5}$$

Putting Eqs.(3) and (4) into Eq.(5), after elementary operations this expression can be written as

$$< \Delta A > = \sum_{i=1}^{M} \{q_I\}\{\Delta A_I\} + \sum_{I=1}^{M} <q_I'>\{\Delta A_I\} + \sum_{I=1}^{M} \{q_I\}<A_I'> + \sum_{I=1}^{M} <q_I'><A_I'>, \tag{6}$$

where the first term is equal to zero, if only $\{q_I\}$ and $\{\Delta A_I\}$ are calculated from the same reference period. The remaining three terms can be interpreted as follows:

- $\Sigma <q'_I> \{\Delta A_I\}$ is the part of the $<\Delta A>$ anomaly due to anomalous frequency distribution of macrotypes. This term of *circulation* origin is henceforth referred as *C*.
- $\Sigma \{q_I\} <A'_I>$ is the part of anomaly, directly not influenced by frequencies of macrotypes. This *physical* or *non-circulation* term, *P* will be discussed in detail below.
- $\Sigma <q'_I> <A'_I>$ is the term (*M*) due to *mixed* influence of both circulation and non-circulation (physical) origin.

So the anomaly for a given period is separated into 3 terms:

$$< \Delta A > = C + P + M . \tag{7}$$

Information contained by the distribution of macrosynoptic types, related to the expected use of GCM-outputs (see Introduction) is included in term *C* and partly in term *M*. The physical (non-circulation) term, on the other hand, is determined by processes of at least three roots.

The *first* one is the initial large-scale anomaly, compared to the climatic mean pattern of the given macrotype, which is not great enough to select this pattern into a different class. This large-scale source of term *P* can appear tendentiously parallel to climate variations and changes. The *second* source of term *P* can be originated in the local anomalies of the underlying surface (heat and moisture content) that of course might indirectly be influenced by the sequence of macrotypes within their fixed frequency distribution. *Thirdly*, term *P* may also contain the effects of scales not resolved by the horizontal grid-structure of the classification, or those connected to peculiarities of the

actual vertical profiles, which are not represented by the one vertical level, used in the classification.

The aim of our calculations is to estimate the relative weights of these terms in local climate anomalies. To do so, day-by-day sequences of meteorological elements and of actual macrotypes are needed. The method described above can be used for any individual period of interest, but we try to apply it independently of *episodic* particularities of the periods, which they are calculated for. Therefore anomalies of the whole longer-term period (see *Section 2.2*) are selected into 5 groups as extremely positive (++), positive (+), medium (=), negative (-) and extremely negative (--) ones, representing 20−20% of the frequency distribution in the arranged sample of local climate anomalies (see *Section 2.3*). Calculation of terms in Eq. (7) is performed for separate months in the groups, and results are averaged within the groups thereafter.

2.2 The macrosynoptic classification

The classification of macrosynoptic types to be applied can be chosen from a finite set of objective or expert-defined classifications covering either the whole Hemisphere or just the area, related to the given locality. There are, however, some considerations motivating the choice of classification.

First, the separation method requires a macrosynoptic classification in a limited area, because local weather anomalies and macrotypes should be considered synchronously. On the other hand, it would not be reasonable to have a horizontal resolution for the data base of classification, which were higher than in the GCM-s simulating the circulation patterns.

Ambrózy et al. (1983,1984) have published an objective macrosynoptic classification, fulfilling these two criteria, which is based on cluster-analysis ("K-means", see e.g. *Anderberg*, 1973) of the 500 hPa geopotential fields. In this study the Atlantic-European region is represented by 80 grid-points on a 5°x10° geographical grid (*Fig. 1*). The initial classification, i.e. the typical geopotential patterns, forming the cluster-centers in the 0-th step of classification was the *Hess* and *Brezowsky*'s (1969) classification (HB), being uniform in each season. However, *Ambrózy et al.* (1983, 1984) established that frequencies of the objective versions of HB-types exhibit definite annual variations. Therefore, the classification was fulfilled for all seasons separately, between 1949 and 1972.

Having the macrotypes already defined, the identification of individual days were continued also after 1972, but it was terminated in 1985 for technical reasons. In our study, macrosynoptic codes for the period 1951-1980 are used.

Numbers and average durations of macrotypes, maximum and minimum external distances between them, and also standard deviations (i.e. mean internal distances) of the macrotypes averaged to one grid-point are presented in *Table 1*, compiled according to the original papers. Short average durations

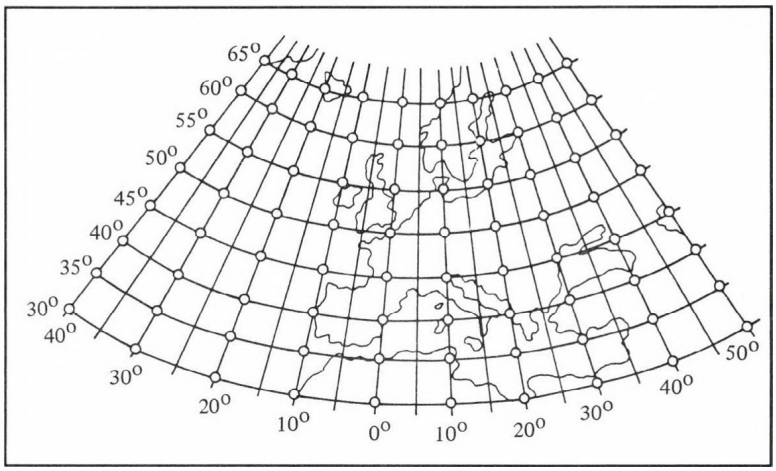

Fig. 1. The Atlantic-European sector and the 5°x10° grid of the applied macrosynoptic classification (from *Ambrózy et al.*, 1983).

of macrotypes suggest that the applied horizontal and vertical resolutions are fine enough to produce macrosynoptic patterns having the same average duration as the local weather. Advantages of the objective classification, as compared to the initial HB, can be realized (*Ambrózy et al.*, 1983) if comparing the average internal distances presented in Table 1 (8.0−10.3 gpm) with those of the original HB catalogue (14.4 gpm).

There are three advantageous properties of the applied classification, that are thought to be important for the adequate separation. First, *objectivity of the classification and day-by-day recognition* of the patterns assures the separation against (expert-induced) systematic distortions in the estimation of the terms in Eq. (7). Second, *equivalent importance of each 80 grid-points* (in contrast to

Table 1. Characteristics of the applied objective macrosynoptic classification

	Number of macrotypes	Mean duration of macrotypes (days)	Average internal distance (gpm)	Distance between macrotypes (gpm)	
				Maximum	Minimum
Winter	17	2.4	10.3	25	4
Spring	19	2.5	9.3	26	8
Summer	8	3.5	8.0	15	6
Autumn	15	2.7	9.6	26	9

classifications which emphasize one certain country or region) is crucial to assure the independence of macrosynoptic classes of the weather in the investigated locality, having influence only in a few grid-points.

Third, the classification *considers the absolute value of geopotential*, not only the qualitative features of the pattern. This makes it possible to distinct qualitatively similar situations with different temperatures (relative geopotentials) in the troposphere.

2.3 Grouping the anomalies in local climate elements

The method of separation can be applied for the whole Atlantic-European region and for all climate elements. Of course, results and conclusions concerning the use of GCM-outputs in the suggested way, may highly depend on the area and element for which the separation is carried out.

In the following we present the results of separation for monthly *temperatures* and *precipitation* anomalies for *Kecskemét*, Hungary (47°N 20°E) located in a representative plain area. This point is in the middle of the north-south, and at the eastern 2/3 of the west-east extension of the area, used for the macrosynoptic classification.

Monthly anomalies of both meteorological elements are divided into five groups, representing 20−20% of the empirical distribution, according to their sign and severity, as suggested in *Section 2.1*. So, 6−6 months from the samples containing 30 years between 1951 and 1980 are selected for each anomalygroup. Boundary values between the neighboring anomaly-groups are presented in *Figs. 2* and *3* for temperature and precipitation, respectively.

3. Results

In the following only four anomaly groups are analyzed, as for the middle group (little or no anomalies) signs of the weights are often the opposite as the anomalies themselves.

3.1 Temperature

Results of separation for the extreme categories (++ and −−) are presented in *Fig. 4*. It can be seen that relative weights of circulation, physical and mixed components have definite annual cycles. Absolute dominance of the physical component in the warm months and approximate equilibrium among the components in the cold months can be established, except for November–December in the (−−) anomalies. All components exhibit the same sign as the anomalies themselves, except for June. Main features of distributions in the (++) group are nearly the same as in the (−−) group.

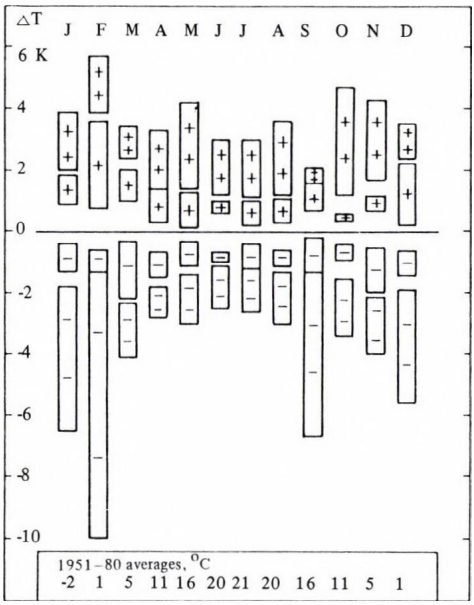

Fig. 2. Groups of monthly mean temperature anomalies (ΔT) at Kecskemét, Hungary. Average rounded values in °C are indicated at the bottom.

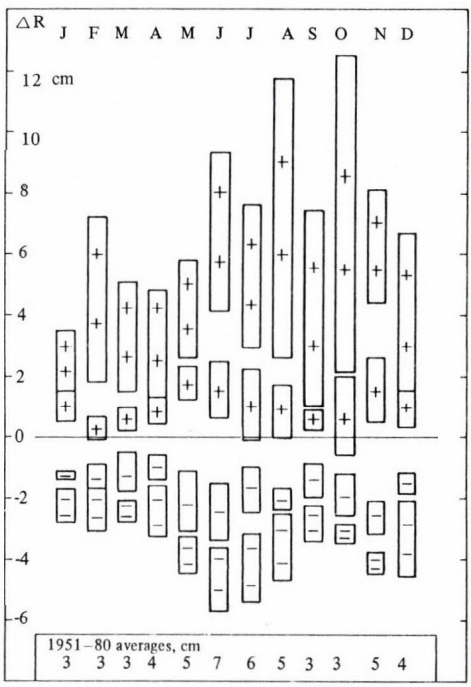

Fig. 3. The same as Fig. 2 for precipitation. Rounded averages in cm/month.

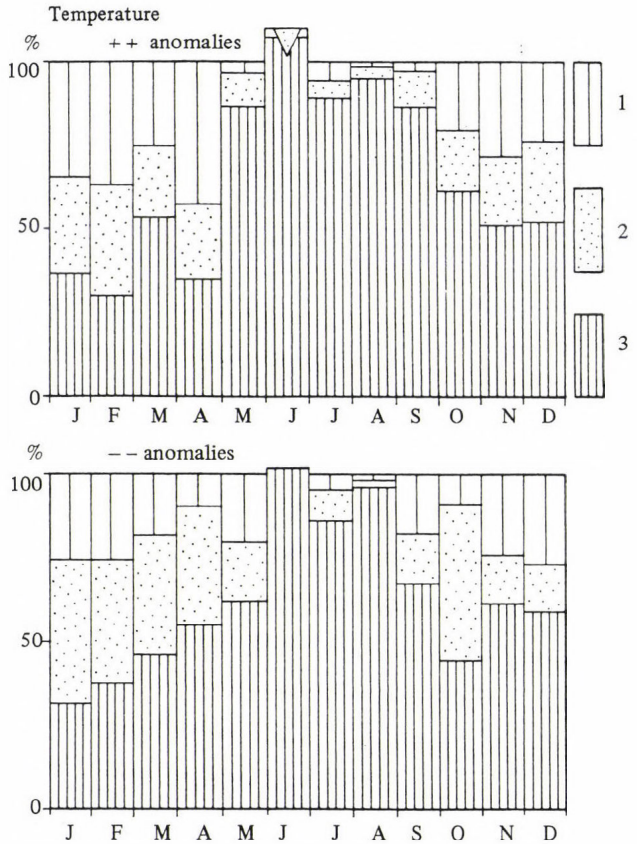

Fig. 4. Proportion of the circulation (1), mixed (2) and physical (3) terms in groups of extremely warm (+ +) and extremely cold (– –) anomalies of temperature at Kecskemét, Hungary. Triangles indicate terms of opposite sign.

To compare the extreme anomalies with moderate (+ and –) ones, seasonal and annual mean weights of the different components, averaged from their initial monthly values, are demonstrated in *Table 2*. The most plausible feature of these numbers is that the difference between relative weights in the different anomaly-groups are small. The dominance of the physical term (P) over the circulation (C) is unambiguous, even in winter. Thus, this is not only a feature of extremities, but a more general characteristic of climate in the given location. The mixed component (100-P-C%) has also just a secondary role (2–23% in annual averages).

3.2 Precipitation

The separation for the two extreme anomaly groups is presented in *Fig. 5*. There are considerable differences between the (––) and (+ +) groups, both in the terms and their annual course. (The sequence of displaying the anomaly

Table 2. Proportion of the physical (P) vs. circulation (C) terms in the temperature anomalies expressed in percents for the different seasons and anomaly groups (Kecskemét, Hungary): ++ extremely warm, + moderately warm etc. groups. The central (40–60%) group is omitted.

Temperature	DJF	MAM	JJA	SON	Year
	C/P	C/P	C/P	C/P	C/P
++	28/40	18/58	0/97	17/66	16/65
+	8/53	18/51	30/118	7/104	16/82
–	25/34	21/52	16/72	9/82	18/60
––	26/42	16/54	2/94	17/57	15/62

groups of different signs is changed with respect to the common appearance of positive temperature with negative precipitation anomalies, and vice versa.) For extreme negative anomalies (––), the physical component has a well defined annual course with a slight dominance (approx. 60%) in summer and a rather minor role in winter. The circulation term has a considerable role (40–50%) in the majority of months, except for December with very high, and for February and August with low weights. For the extremely high precipitation (++) group, a slight uneven dominance of physical components can be established, with no definite annual cycle. The circulation term plays little role in this group. The mixed term is somewhat more important, than in case of the temperature (16–36% in annual mean for the different groups). Synchronism in the sign of the three components can also be recognized, with few exceptions.

For moderate anomalies, the seasonal and annual averages are demonstrated in *Table 3*, together with those for the extreme groups. The relative weights are different for different seasons and for groups of the same strength, but different signs, especially in winter and spring. The most important feature, however, is that no great differences in (++) vs. (+) or in (––) vs. (–) groups can be identified.

4. Discussion

In the presented calculations, regarding to Kecskemét, Hungary, the most important conclusion is the relatively minor role of the circulation term, except for the low precipitation anomalies. The annual course of this term is in broad coincidence with one's *a priori* expectations, as the latter can also be confirmed

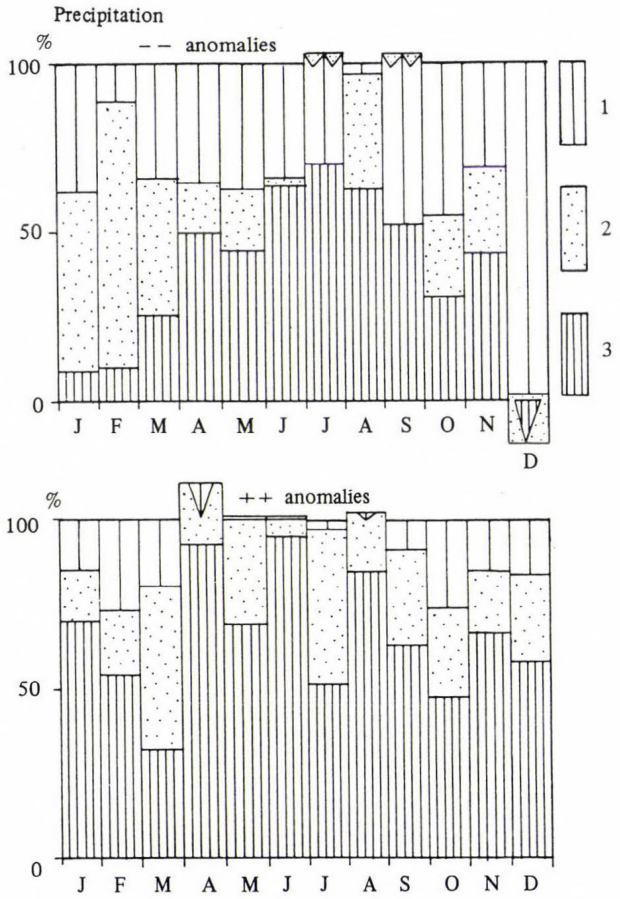

Fig. 5. The same as Fig. 4 for precipitation (e.g. – –: extremely dry).

by Table 1. Here the number of macrotypes in summer is the less in the year, and their "distance" (i.e. mean gpm difference) has also a minimum. Thus, the less the difference between the macrotypes is, the lower part of the anomalies are expected to be attributed to anomalous frequency distribution of the macrotypes.

It is impossible, however, to consider this circulation term as the maximum information contained by a series of macrotypes, because the succession of macrotypes is not taken into account by the separation. E.g. cool and wet westerlies at the beginning of the period (in summer), followed by warm and dry anticyclones could cause a much different monthly anomaly than the opposite case, although the frequency distribution of the investigated period would be the same. Effects, induced by the circulation on previous days are registered in the physical term, implicitly (see explanations of this term, in *Section 2.1*). Therefore, the approach, suggested by *Matyasovszky et al.* (1992) and *Bogardy et al.* (1992), has a reasonable physical background. Thus, it

Table 3. The same as Table 2 for precipitation: – – extremely dry, etc.

Precipitation	DJF C/P	MAM C/P	JJA C/P	SON C/P	Year C/P
– –	77/2	24/4	1/66	42/42	36/38
–	74/–16	34/30	–3/71	16/59	30/34
+	20/66	–3/93	5/65	39/53	15/69
+ +	19/61	3/65	0/77	17/59	10/65

might be worth following the sequence of macrotypes (not their frequencies only), despite the sample problems arising in connection with the more conditions considered.

The seasonal objective classification applied in this study has several advantages detailed in *Section 2.2*, but it is not proven that this were the optimal one. The separation of time averages can also be completed by applying other macrosynoptic classifications, investigating how the results are specific to the applied classification. An alternative to the applied one might be the classification, introduced by *Péczely* (1957, 1983). This, not objective classification represents smaller scale (Europe with a special attention to Hungary), but it has probably more narrow conditional distributions for the weather elements in Hungary.

Our study has been dedicated to an empirical investigation in relation to the application of GCM-outputs. This mixed, empirical-dynamical approach relies on the assumption that the response of the regional climate to a changing global flow, due either to interannual climate variability or to the longer-term changes, is the same in both cases. This assumption, however, remains unproven for any combination of circulation patterns related to the future with conditional distributions of the present climate. This uncertainty should always be taken into consideration, relying on regional climate scenarios based on this combination.

Acknowledgements – The author thanks *Ms. Judit Bartholy* for making the catalogue of the applied macrosynoptic classification and also the conditional climatological data available, and *Ms. Márta Korándi* for programming the calculations on an IBM-360 computer. Preparation of this paper was partly supported by contract OTKA-443 with the Hungarian Academy of Sciences.

References

Ambrózy, P., Bartholy, J. and *Gulyás, O.*, 1983: Determination of seasonal macro-synoptic types for the Atlantic-European region by cluster-analysis (in Hungarian).

OMSZ Kisebb Kiadványai, No. 39, Budapest.

Ambrózy, P., Bartholy, J. and *Gulyás, O.*, 1984: A system of seasonal macrocirculation patterns for the Atlantictic-European region. *Időjárás 88*, 121-133.

Anderberg, M.R., 1973: *Clusteranalysis for Applications*. Academic Press, New York.

Bogardi, I., Matyasovszky, I., Bardossy, A. and *Duckstein, L.*, 1992: Estimating space-time local hydrological quantities under climate change. In *Proc. 5th Int. Meeting on Statistical Climatology*, 22-26 June, 1992 Toronto, Canada, 95-99.

Cohen, S.J. and *Allsopp, T.R.*, 1988: The potential impacts of a scenario of CO_2-induced climatic change on Ontario, Canada. *J. Climate 1*, 669-681.

Giorgi, F., Marinucci, M.R. and *Visconti, G.*, 1990: Use of a limited area model nested in a general circulation model for regional climate simulation over Europe. *J. Geophys. Res. 95*, 18413-18431.

Grotch, S.L. and *MacCracken, M.C.*, 1991: The use of general circulation models to predict regional climate change. *J. Climate 4*, 286-303.

Hess, P. and *Brezowsky, H.*, 1969: Katalog der Grosswetterlagen Europas. *Berichte des Deutschen Wetterdienstes Bd. 15*, N. 113, Offenbach.

Karl, T.,W., Wang, W.-C., Schlesinger, M.E., Knight, R.W. and *Portman, D.*, 1990: A method of relating general circulation model simulated climate to the observed local climate. Part I: Seasonal statistics. *J. Climte 3*, 1053-1079.

Kim, W.J., Chang, T., Baker, N.L., Wilks, D.S. and *Gates, W.L.*, 1984: The statistical problem of climate inversion: Determination of the relationship between local and large-scale climate. *Mon. Wea. Rev. 112*, 2069-2077.

Klein, W.H. and *Yang, R.*, 1986: Specification of monthly mean surface temperature anomalies in Europe and Asia from concurrent 700 mb monthly mean height anomalies over the Northern Hemisphere. *J. Climatology 6*, 463-484.

Matyasovszky, I., Bogardi, I., Bardossy, A. and *Duckstein, L.*, 1992: Hydroclimatological modeling of droughts under climate change. In *Proc. 16th European Regional Conference of ICID.*, 21-27 June, 1992, Budapest, Hungary, 239-250.

Mika, J., 1991: Regional features of a stronger global warming over Hungary (in Hungarian). *Időjárás 95*, 265-278.

Mitchell, J.F.B., Manabe, S., Tokioka, T. and *Meleshko, V.*, 1990: Equilibrium climate change. In *IPCC WG-1 Report, WMO-UNEP*, 139-174 .

Péczely, G., 1957: Grosswetterlagen in Ungarn. *Kleinere Veröffentlichungen der Zentralanstalt für Meteorologie*, No. 30., Budapest.

Péczely, G., 1983: Catalogue of the macrosynoptic types for Hungary (1881-1983) (in Hungarian). *Meteorológiai Tanulmányok* 53, OMSZ, Budapest.

von Storch, H., Zorita, E. and *Cubasch, U.*, 1991: Downscaling of global climate change estimates to regional scales: An application to Iberian rainfall in wintertime. *Max Planck Inst. Meteor. Rept.* No. 64, Hamburg, June 1991.

Werner, P.C., 1992: On the relationship between the atmospheric circulation in the Atlantic-European area and some seasonal meteorological parameters in Central Europe. In *Proc. 5th International Meeting on Statistical Climatology*, 22-26 June, 1992, Toronto, Canada, 161-164.

Wigley, T.M.L., Jones, P.D., Briffa, K.R. and *Smith, G.*, 1990: Obtaining sub-grid scale information from coarse-resolution general circulation model output. *J. Geophys. Res. 95 (D2)*, 1943-1953.

IDŐJÁRÁS

Quarterly Journal of the Hungarian Meteorological Service
Vol. 97, No. 1, January–March 1993

Trace metal concentrations in atmospheric precipitation over Hungary[1]

E. Mészáros*, A. Molnár*, Zs. Horváth and A. Lásztity****

* *Department of Analytical Chemistry, University of Veszprém, H-8201 Veszprém, P.O.Box 158, Hungary*
** *Institute of Inorganic and Analytical Chemistry, Eötvös Loránd University, H-1518 Budapest, P.O.Box 112, Hungary*

(Manuscript received 11 January 1993; in final form 5 April 1993)

Abstract—The aim of this paper is to present the concentration of ten trace metals in atmospheric precipitation waters. Precipitation samples were taken by means of a wet-only collector at a regional background site in central Hungary. The water samples were analyzed by the inductively coupled plasma atomic emission spectroscopy (ICP-AES). The results obtained are discussed and compared to those published in the literature, as well as to emission information available.

Key-words: chemical composition of precipitation, wet deposition, toxic metals, Hungary.

1. Introduction

The study of the chemical composition of precipitation provides useful information for estimating the trace substance concentration and self-cleaning capacity of the atmosphere. On the other hand, such an investigation is of interest to determine the impact of atmospheric pollution on terrestrial and aquatic ecosystems.

For these reasons the chemical composition of atmospheric precipitation has been widely studied under several geographic conditions (see e.g. *Mészáros*, 1981; *Warneck*, 1988) including the central-eastern part of Europe (e.g. *Horváth* and *Mészáros*, 1984; *Malissa et al.*, 1984; *Moldan et al.*, 1987). However, in the latter studies only the concentration of inorganic ions was determined. With the exception of some alkali and alkaline earth metals, the

[1] Sponsored by the National Foundation for Scientific Research (OTKA, N° 345).

level of trace elements was not detected in spite of their importance in ecological studies. In this paper the concentrations of ten metals in precipitation are presented from the analyses of daily samples collected in the middle of Hungary under rural conditions (K-puszta station, ϕ=46°58'N λ=19°33'E H=130 m) by a wet-only sampler. These new measurements were possible through the application of the inductively coupled plasma atomic emission spectrometry (ICP-AES).

2. *Analytical technique*

Precipitation samples were acidified with HNO_3 down to pH=2 at the station immediately after collection. The samples were then transported to the laboratory and submitted to a preconcentration procedure. For this purpose a microcolumn filled with iminodiacetic acid/ethyl cellulose ion (IDAEC) exchanger was used. The samples were buffered with 1M ammonium acetate and pumped through the column in a flow system. The trace metals thus collected in the column were eluted by injection with 100 μL of 2M HNO_3 and introduced into the plasma torch of the ICP-AES device.

Fig. 1 shows the schematic diagram of the system used. Data obtained with this system show that in all cases the column uptake is directly proportional to the metal concentration in solution. Results also indicate that the reproducibility of the preconcentration process is better than 5 % (for further details including calibration see *Horváth et al.*, 1992).

In seven samples the concentration of cadmium, manganese and lead was also determined simultaneously by graphite furnace atomic absorption spectrometry widely used in environmental studies. Data gained by the two methods are in good agreement. On the basis of seven samples the ratio of the concentration measured by ICP to that detected by atomic absorption spectrometry is 1.1, 0.99 and 1.2 for Cd, Mn and Pb, respectively. The higher ratio

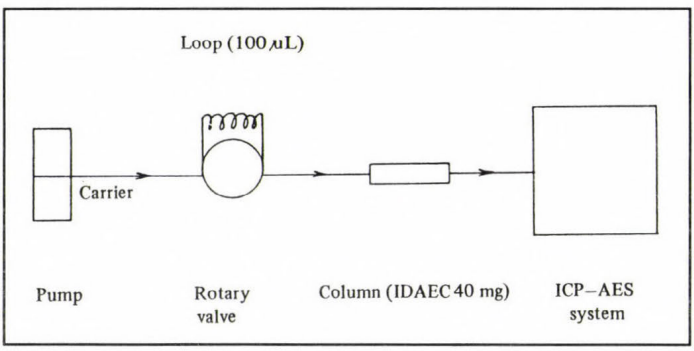

Fig. 1. Schematic diagram of the preconcentration (IDAEC) and analysis (ICP-AES) system.

for Pb is caused by differences when the concentrations are lower than 10 μgL^{-1}. Thus, it can be concluded that in the future for Pb a higher preconcentration factor should be used.

Finally we note that the analysis of calcium and magnesium was found to be possible by ICP-AES without preconcentration due to their relatively high concentration. However, in this paper the concentration of these elements is not discussed since similar results were obtained as in the case of our previous studies (*Horváth* and *Mészáros,* 1984).

3. Concentrations

The average concentrations of ten metals calculated by weighing the individual values with precipitation amount are given in the first column of *Table 1*. These data were obtained on the basis of the analysis of 46 daily samples collected between 1 July and 31 December, 1991. In the second column of the table the detection limits of the analyses are also tabulated. It can be seen that the detection limits are significantly lower than averages, except for vanadium for which the ratio of the average to the detection limit is only slightly higher than two. This means that vanadium data must be considered with some caution.

It should be noted that the scatter of data around the averages is rather large as the third line of Table 1 shows. This is due to the inverse relationship between elemental concentration and precipitation amount. Further analyses are necessary, however, to determine this relationship on solid statistical basis.

In the fourth column of Table 1 the average concentrations compiled for rural areas by *Galloway et al.* (1982) are tabulated. As in our case these data refer to regional conditions, not directly influenced by local anthropogenic emissions. The comparison of these data with our results indicate that the values measured in Hungary are rather close to word-wide average concentrations, with the exception vanadium. The detection of the latter is somewhat questionable, as was mentioned above. *Barrie et al.* (1987) noted that the trace metal concentrations reported by Galloway and his associates are unreliable because of possible sample contamination. For this reason the values reported by *Ross* (1986) for Southern Sweden are also included in Table 1 (last column). In the Swedish study, like in our case, proper precautions were taken to avoid sample contamination (samplers were acid-washed). Although for four metals (Cu, Zn, Pb and Cd) Swedish concentrations are smaller than our values, the two data sets are still comparable. It is speculated that the observed differences between Southern Sweden and Hungary are real and due to different environmental conditions. Overall we conclude that Hungarian concentrations reported in this paper do not differ significantly from concentrations observed in other regional background areas of the world.

Table 1. Concentration of metals in precipitation in Hungary and over other regions. The values are expressed in $\mu g\ L^{-1}$

Element	Concentration	Detection limit	Range of concentration	Rural average[1] word	Southern Sweden[2]
Ti	0.76	0.1	<0.1 – 3.8	–	–
V	1.9	0.9	<0.9 – 5.4	9.0	–
Mn	7.0	0.9	<0.9 – 41	5.7	6.4
Fe	70	2.0	13 – 360	–	–
Co	0.85	0.1	<0.1 – 3.6	0.75	–
Ni	1.7	0.1	<0.1 – 16	2.4	–
Cu	6.7	0.6	<0.6 – 157	5.4	1.4
Zn	46	0.9	0.8 – 96	36	16
Pb	8.9	0.4	<0.4 – 160	12	8.8
Cd	0.52	0.1	0.24 – 2.9	0.50	0.14

[1] *Galloway et al.* (1982)
[2] *Ross* (1986)

4. Scavenging coefficients and wet depositions

During the year when precipitation samples were collected the elemental composition of the aerosol particles was also measured (*Molnár et al.*, 1993). These measurements were carried out by the PIXE analysis of aerosols captured on Nuclepore filters. This makes it possible to calculate the scavenging coefficients defined as the ratio of the concentration of a given element in precipitation to that in the aerosol phase. The results obtained are listed in the first column of *Table 2.* Except for titanium the coefficients are close to 10^6 proposed as a general value for different elements by *Pacyna et al.* (1984).

The climatic average of annual precipitation amount measured in the region of our sampling station is equal to 518 mm. Using this figure and the average concentrations presented in Table 1, the wet deposition values can be calculated. The deposition rates (in mg $m^{-2}\ yr^{-1}$) are given in the second column of Table 2, while the data in the third column of the table show an extrapolation to total area of Hungary. Deposition values are high in particular for iron and zinc. For these elements the annual deposition is of the order of tens of mg $m^{-2}yr^{-1}$. In the case of iron the high deposition is at least partly caused by

Table 2. Scavenging coefficients ($x10^5$), wet deposition rates (in mg m^{-2} yr^{-1}), total wet deposition and emissions (both in t yr^{-1}) of trace metals in Hungary

Element	Scavenging coefficient	Deposition rate	Hungarian deposition	Emission[1]
Ti	0.46	0.39	36	–
V	5.9	0.98	92	389
Mn	14.3	3.6	336	160
Fe	2.7	36	33620	–
Co	3.3	0.44	41	24
Ni	5.7	0.89	83	162
Cu	7.1	3.5	323	509
Zn	12	24	22416	280
Pb	4.7	4.6	430	888
Cd	–	0.27	25	8

[1] *Pacyna et al.* (1984)

the contribution of crustal sources. This is shown by the enrichment factor of iron in aerosol samples (*Molnár et al.*, 1993) collected at the same station. However, the high deposition of Zn is at least partly due to anthropogenic sources (e.g. fossil fuel combustion, metal industry, refuse incineration) which are located mainly outside of Hungary as indicated by long-range transport model calculations (*Molnár et al.*, 1992). Further studies are needed, however, to determine the reasons for this relatively high Zn deposition.

It should be noted that although cadmium deposition is numerically low, the calculated Cd depositions might be dangerous from an environmental point of view due to the high toxicity of this element. Thus, according to *Galloway et al.* (1982) cadmium is toxic for aquatic organisms at concentrations as low as 0.2 μg L^{-1}, which is less than half of the average concentration measured (see Table 1). Pb wet deposition is important, but it is lower than the average value reported for Hungary for the period between 1984 and 1988 (*Bozó* and *Horváth*, 1992). This decrease is obviously caused by the use of gasolines with low lead content in recent years, outside and inside of the country.

Finally, in Table 2 (last column) emission values estimated by *Pacyna et al.* (1984) for Hungary are also given. It can be seen that for V, Ni, Cu and Pb the

emissions are higher than depositions. This can be probably explained by the fact that dry deposition is not included into the study. The situation is quite different for the other four elements for which the emissions are tabulated. For Mn this might be due to the contribution of crustal sources to the deposition, while for Co and Cd long-range transport is the probable origin. However, in the case of Zn this explanation does not hold since the wet deposition measured is much higher (about eight times) than the emission calculated by *Pacyna* and his co-workers. This obviously means that further, more reliable emission calculations are needed. Furthermore the more appropriate determination of the wet deposition by using several sampling sites in the country is necessary.

5. Aims of further research

On the basis of the above discussion we conclude that for a reliable calculation of the budget of different metals in the air over Hungary, the following items should be included into the study:

(a) reconsideration of emission values given for Hungary by *Pacyna et al.* (1984);
(b) estimation of the dry depositions for the country and
(c) determination of the wet deposition on the basis of samples collected at several sites.

Thus, we will continue the project in these directions.

References

Barrie, L.A., Lindberg, S.E., Chan, W.H., Ross, H.B., Arimoto, R. and *Church, T.M.*, 1987: On the concentration of trace metals in precipitation. *Atmos. Environ. 21*, 1133-1135.

Borbély-Kiss, I., Bozó, L., Koltay, E., Mészáros, E., Molnár, Á. and *Szabó, Gy.*, 1991: Elemental composition of aerosol particles under background conditions in Hungary. *Atmos. Environ. 25A*, 661-668.

Bozó, L. and *Horváth, Zs.*, 1992: Atmospheric concentration and budget of lead and cadmium over Hungary. *Ambio 21*, 324-326.

Galloway, J.N., Thornton, J.D., Norton, S.A., Volckok, H.L. and *McLean, R.A.N., 1982:* Trace metals in atmospheric deposition: a review and assessment. *Atmos. Environ. 16*, 1677-1700.

Horváth, L. and *Mészáros, E.*, 1984: The composition and acidity of precipitation in Hungary. *Atmos. Environ. 18*, 1843-1847.

Horváth, Zs., Lásztity, A. and *Varga, I.*, 1992: The role of spectrochemical analysis in the determination of the composition of atmospheric precipitation and aerosol samples in remote environment. *Microchem. J. 46*, 130-135.

Malissa, H., Puxbaum, H., Pimminger, M. and *Nikoopour, A.*, 1984: Untersuchungen des Nährstoffeintrages in der Neusiedler

See aus der Atmosphäre. In *Forschungsbericht 1981-1984.* Bundesministerien für Wissenschaft und Forschung, 41-89.

Mészáros, E., 1981: *Atmospheric Chemistry.* Elsevier, Amsterdam.

Moldan, B., Veselý, M. and *Bartoňova, A.*, 1987: Chemical composition of atmospheric precipitation in Czechoslovakia 1976-1984-I. monthly samples. *Atmos. Environ. 21,* 2383-2396.

Molnár, A., Bozó, L., Mészáros, E. and *Harris, J.M.*, 1992: Long-range transport of different elements in atmospheric aerosols: the case of Hungary. In *Nucleation and Atmospheric Aerosols* (eds.: *N. Fukuta* and *P.E. Wagner*), A. Deepak Publ., Hampton, Virginia, 473-480.

Molnár, A., Mészáros, E., Bozó, L., Borbély-Kiss, I., Koltay, E. and *Szabó, Gy.*, 1993: Elemental composition of atmospheric aerosol particles under different conditions in Hungary. *Atmosheric Environment* (submitted).

Pacyna, J.M., Semb, A. and *Hanssen, J.E.*, 1984: Emission and long-range transport of trace elements in Europe. *Tellus 36B,* 163-178.

Ross, H.B., 1986: The importance of reducing sample contamination in routine monitoring of trace metals in atmospheric precipitation. *Atmos. Environ. 20,* 401-405.

Warneck, P., 1988: *Chemistry of Natural Atmosphere.* Academic Press, New York.

IDŐJÁRÁS

Quarterly Journal of the Hungarian Meteorological Service
Vol. 97, No. 1, January–March 1993

Simulation of soil moisture dynamics

G. A. Georgiev and **V. A. Alexandrov**

Institute of Meteorology and Hydrology,
Bulgarian Academy of Sciences, Trakia Blvd.66, Sofia, Bulgaria

(Manuscript received 18 June 1992; in final form 22 March 1993)

Abstract—One of the most important factors determining the productiveness of the plants is the soil moisture. The knowledge of wetting conditions is helpful in planning of meliorative activities. The paper presents a model for calculating the dynamics of soil moisture during the vegetation period between wilting point and fully saturated soil. The blocks of evapotranspiration calculation with using a modified Penman-Monteith equation, precipitation assimilation and soil moisture movement in different layers are concerned. Data of comparison between measured and simulated values of soil moisture content under the maize plants are presented. Daily average meteorological data of air temperature, air humidity deficit, sunshine duration and precipitation quantity are used for calculating of soil moisture profile.

Key-words: Penman-Monteith equation, effective rainfall, agrometeorological modelling.

1. Introduction

The moisture is one of the irreplaceable life factors for agricultural crops. The soil moisture is practically the single water source of plants. The water takes part in the next processes: photosynthesis, thermoregulation of the crop and its mineral nutrition. Different values of soil moisture are observed from year to year in many regions and areas all over the world. The dependence between the yield and the soil moisture is very favourable for assessment of the expected yield.

2. Analysis and methods

The water balance equation, applicable to every soil layer, is basic part of the our model

$$W_i^{j+1} = W_i^j - \lambda E_i^j + q_{i-1}^j - q_i^j, \tag{1}$$

where W_i^j, W_i^{j+1} moisture content of i-th soil layer in the j day and the next $j+1$ day; q_{i-1}^j, q_i^j amount of passed water through i-th layer's boundary per day; λE_i^j evapotranspiration. We suppose that the plant roots reach 100 cm soil depth, arbitrarily divided into ten discrete layers (i=1,2,3,..,10). We use an eleventh layer (100–110 cm) too, whose moisture content is constant. The formula, for determination of water flux through the soil layers, is established by means of the theory describing the water streams in unsaturated soil (*Sirotenko*, 1981)

$$q_i^j = \sqrt{K_i^j K_{i+1}^j} \left[\left(\frac{\psi_{si+1}^j - \psi_{si}^j}{h_s} \right) + 1 \right], \tag{2}$$

where K_i^j water conductivity of the soil, ψ_{si}^j soil moisture pressure, h_s thickness of the soil layer. The soil moisture pressure during the period between wilting point and fully saturated soil was presented by *Mitchurin* (1975) with empirical equation

$$\psi_{si}^j = 15 \exp\left(- 7.76 \frac{W_i^j - W_i^{wp}}{W_i^{fs} - W_i^{wp}} \right), \tag{3}$$

where ψ_{si}^j water potential (10^5 Pa), W_i^{fs}, W_i^{wp} moisture of fully saturated soil and wilting point at i-th layer. When the soil saturation approximates 1, $\psi_{si}^j \to 0$, and when it equals to 0, $\psi_{si}^j = 15$. For the connection between hydraulic conductivity and soil moisture the following relationship (*Sirotenko*, 1981), is used

$$K_i^j = \bar{K}_{oi} \left(W_i^j - \frac{W_i^{wp}}{W_i^{fs} - W_i^{wp}} \right)^F, \tag{4}$$

where $\bar{K}_{oi}$ hydraulic conductivity (filtering coefficient) of saturated soil, F parameter. Using Karman–Kozen's formula (*Mitchurin*, 1975) we obtain

$$\bar{K}_{oi} = \frac{K_o \left(0.01\, W_i^{fs}\right)^3}{\left(W_i^{wp}\right)^2 \left(1 - 0.01\, W_i^{fs}\right)^2}, \tag{5}$$

where K_o empirical parameter.

The Penman-Monteith equation (*Thompson et al.*, 1981) provides a rational, physically-based procedure for calculating the water loss from any surface. The equation is

$$\lambda E = \frac{\Delta (R_N - G) + \rho c_p (e_s - e)/r_a}{\Delta + \gamma (1 + r_s/r_a)}, \tag{6}$$

where E rate of water loss (Kg m^{-2} s^{-1}), Δ rate of change of saturated vapour pressure with temperature (hPa $°C^{-1}$), R_N net radiation (W m^{-2}), G soil heat flux (W m^{-2}), ρ air density (Kg m^{-3}), c_p specific heat of air at constant pressure (1005 J Kg^{-1}), e_s saturation vapour pressure at screen temperature (hPa), e screen vapour pressure (hPa), λ latent heat vaporization ($\approx$ 2465000 J Kg^{-1}), γ psychromatic constant=0.66 for temperatures in deg C and vapour pressures in (hPa), r bulk surface resistance (s m^{-1}), r_a bulk aerodynamic resistance (s m^{-1}). This formula may be written thus as follows

$$\lambda E = - \frac{\Delta (R_{NE} - G) + \rho c_p \delta q (1 + b r_a/\rho c_p)/r_a}{\Delta + \gamma (1 + r_s/r_a)(1 + b r_a/\rho c_p)}, \tag{7}$$

where R_{NE} is R_N calculated assuming $T_o = T_{SCR}$, T_o bulk surface temperature, T_{SCR} screen temperature, ϵ emissivity of surface, $b = 4\,\epsilon\sigma\,(273.1 + T_{SCR})^3$, σ Stefan-Boltzman's constant, δq specific humidity deficit at screen height. This is the combination used in our model.

Prof. *J. L. Monteith* of the University of Nottingham provided constructive suggestion for aerodynamic resistance as the sum of momentum and bluff-body terms (*Choudhury* and *Idso*, 1985)

$$r_a = \frac{\ln^2((z - d)/z_o)}{k^2 u} + \frac{4 \cdot \ln((z - d)/z_o)}{ku}, \tag{8}$$

where k=0.4 the Karman constant, u wind speed at height z, d and z_o are the zero-plane displacement and the roughness height, respectively, calculated from the crop height (H) as: d=0.56H, z=0.13H.

For seasonal crops the surface will range from bare soil, to moderately or densely foliated. Water may be extracted directly from both the soil and the crop, and the surface resistance has to be calculated by taking both these processes into account. The basics scheme is based on suggestion by *Grant* (*Thompson et al.*, 1981) and uses the expression

$$1/r_s = (1 - A)/r_{sc} + A/r_{ss}, \quad (9)$$

where r_{ss} surface resistance of the crop, freely supplied with water, and dense enough for evaporation from the soil to make a negligible contribution, r surface resistance of bare soil (assumed to be 100 s m^{-1} for wet soil), $A=f^L$ (where L leaf area index). *Grant* found that f for barley was about 0.7, and this value has been assumed to apply to all the crops treated by our model. The last Eq. (9) has been derived for daytime conditions, assuming the parallel contributions of soil and crop resistance to their combined resistance to be roughly proportional to the amount of incident radiation which is absorbed by each of them. At night the leaf stomata are closed and the crop resistance r_{sc} is assumed to be the sum of the individual leaf (cuticular) resistances in parallel. These in turn are taken to be directly in parallel to the soil resistance so that

$$1/r_s = 2L/r_{sc}\,(\text{night}) + 1/r_{ss}. \quad (10)$$

A typical leaf resistance when stomata are closed, is about five thousand s m^{-1}, consequently Eq. (10) assumes the next form

$$1/r_s = L/2500 + 1/r_{ss}. \quad (11)$$

It is not possible to justify this last equation convincingly since it ignores the effects of turbulent resistances in the crop canopy. However, evaporation is usually small at night so errors introduced by Eq. (11) will also be small.
From concurrent data of stomatal conductance of sunlit leaves (C_1;mm s^{-1}), leaf water potential (ψ;m) and net radiation (R_N;W m^{-2}) *Choudhury* and *Idso* (1985) derived the empirical relationship

$$C_l = (0.986 + 0.025\,R_N) f_2\,. \quad (12)$$

The function f_2 was proposed by *Fisher* (*Fisher et al.*, 1981)

$$f_2 = 1/(1 + (\psi/q)^p), \quad (13)$$

where q and p are adjustable parameters. The Eq. (12) may be applied only to sunlit leaves. For a wheat canopy, however, all leaves are not likely to be sunlit. If leaf stomatal conductances were measured within various strata of a canopy to account for varied radiation regimes and leaf ages then canopy conductances (g_c) could be obtained as (*Roberts et al.*, 1980; *Choudhury* and *Idso*, 1985)

$$g_c = \sum_{j=1}^{n} L_j C_{lj} = (0.986L + R_N(1 - \tau))f_2, \quad (14)$$

where $j=1$ to n represents canopy strata having a leaf area index of L_j and leaf stomatal conductance of C_{lj}, τ an exponential function (*Denmead* and *Millar*, 1976): $\tau=\exp(-L/(2 \sin \Theta))$, Θ is solar elevation. Now the canopy resistance r_{sc} (s m^{-1}) follows from Eq. (14) as

$$r_{sc} = 1000/g_c. \quad (15)$$

The following plan for accounting the effective precipitation is suggested. At first, the rainfall sums are determined. The rainfall is effective when the daily sum is bigger than 0.2 mm until tasseling (0.9 mm after tasseling). The effective rainfall (*Sirotenko*, 1981), when $R^j \neq 0$, may be presented with equation

$$R_{ef}^j = R^j \left\{ 1 - \left[1 - \left(\frac{W_{fs}^{50} - W_{50}^j}{W_{fs}^{50} - W_{wp}^{50}} \right)^{1.5} \right]^2 \right\}, \quad (16)$$

where R^j, R_{ef}^j measured rainfall sum and effective rainfall sum per day (mm), W_{fs}^{50}, W_{wp}^{50} moisture of fully saturated soil and wilting point at 0–50 cm layer, W_{50}^j current soil moisture. Eq. (16) allows to account the precipitation loss of the soil surface. So, if $W_{50}^j = W_{fs}^{50}$ then $R_{ef}^j=0$, but when $W_{50}^j = W_{wp}^{50}$ then $R_{ef}^j=R^j$.

The procedure describing the precipitation assimilation is organized by the following steps: the effective rainfall sum is added to moisture of the first soil layer. If $(R_{ef}^j + W_i^j) > WW_i$ then the difference $(R_{ef}^j + W_i^j) - WW_i$ is combined with the next soil layer and it is "effective rainfall" for this layer. The procedure is repeated down to tenth soil layer inclusive. If the last layer is fully saturated, the excess water is added to ninth layer. When the ninth layer is saturated too, the excess water is added to eight soil layer etc. – inclusive of the first soil layer.

3. Results and discussion

The model permits to calculate the distribution of soil moisture from 10 cm to 100 cm depth. The root distribution, soil aeration, physical structure of the soil, underground water, water movement in the soil and root age are very

important elements in this model. We assume that the root distribution of maize is reduced according to the exponential law and the root mass decreases with the depth. It is supposed that the capillary water motion from underground water is absent. The means of agrophysical constants describe the soil structure. Dynamics of soil moisture during the vegetation period between wilting point and fully saturated soil is calculated. The values of soil moisture, which were up or down this interval, were equalized to them. In *Figs. 1a, 1b* and *2a, 2b* the comparison between calculated and measured values of soil moisture in the layers 0–10 cm, 30–40 cm, 60–70 cm, 90–100 cm is shown. Used data were measured in agrometeorological station Knezha (43.50°N, 24.08°E), Bulgaria, in 1982. In *Table 1* the monthly average values of the air temperature (T), air humidity deficit (D) and sunshine duration (S) are shown at meteorological station Knezha in the same year. The soil of the experimental field is typical chernozem.

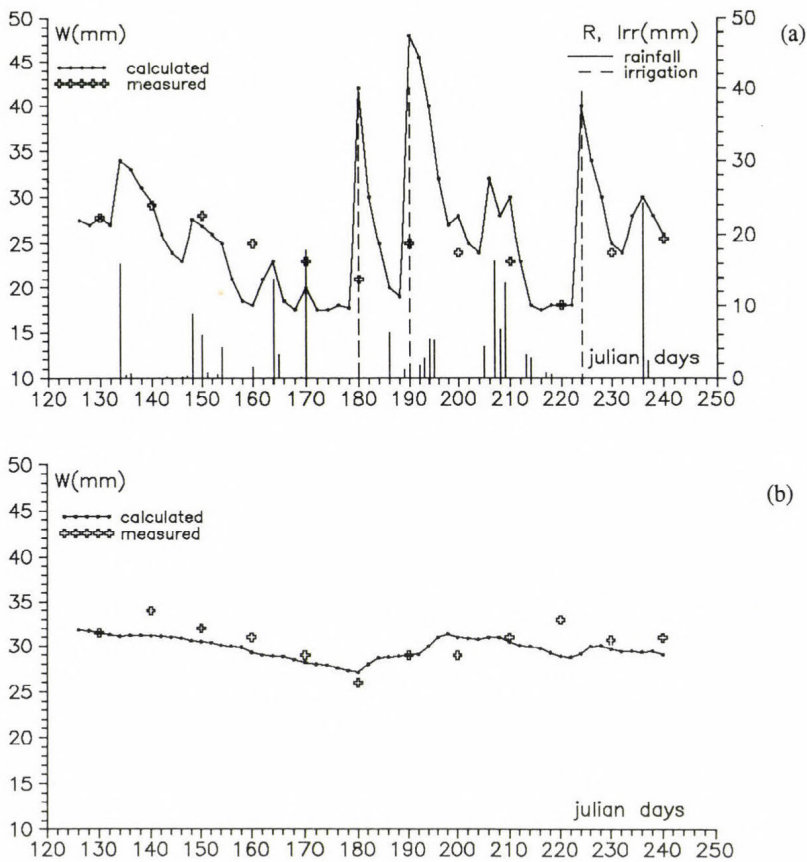

Fig. 1. Comparison between dynamics of calculated and measured soil moisture in layer (*a*) 0–10 cm, (*b*) 30–40 cm under maize.

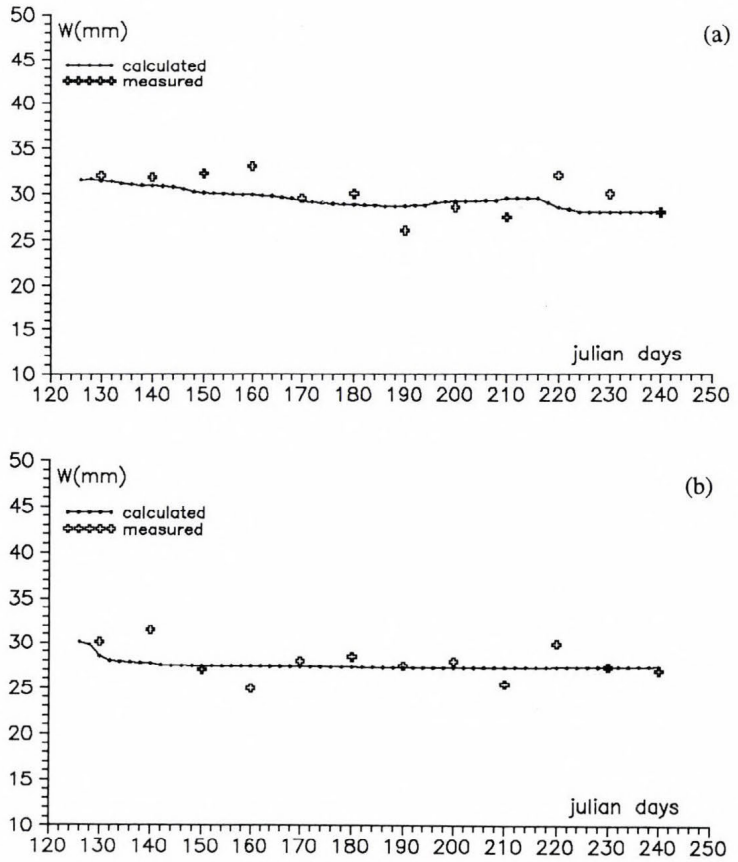

Fig. 2. Comparison between dynamics of calculated and measured soil moisture in layer (*a*) 60–70 cm, (*b*) 90–100 cm under maize.

The calculations for all over the vegetation period without input corrections were done. It is necessary to remark that when the depth increases the instability of soil moisture decreases and there are very small trend in the last layer. In this case, the maximum error is less than 20% and it is within the error's interval of the method of experimental measuring of the soil moisture. The calculated soil moisture is well correlated with atmospheric conditions. The sudden raise of soil moisture in the surface layer coincides with date of irrigation. It is necessary to remark that the maximum deviation of calculated values is observed in these moments. It is explained with the imperfect methods (as the bulk density core method, which we were used) of measuring the soil moisture and the incorrectly chosen place. Assuming the soil moisture below 100 cm as a constant brings to small variation of calculated values and big errors for 90–100 cm layer. Excluding the relationship between the age and the

Table 1. Monthly average values of air temperature (T), air humidity deficit (D) and sunshine duration (S)

	J	F	M	A	M	J	J	A	S	O	N	D
T (°C)	-2.8	-0.7	5.7	14.2	17.0	22.6	22.2	21.3	14.4	8.3	5.8	-0.7
D (hPa)	0.4	0.5	3.5	6.9	7.8	13.8	8.8	10.7	4.2	2.2	2.4	0.6
S (h)	0.6	1.3	5.6	6.5	8.1	10.5	8.4	8.7	4.9	3.8	4.8	1.4

water assimilation abilities of the roots provokes an incorrect calculation of the soil moisture in depth. On the other hand, we consider the soil moisture below 100 cm as a constant.

Nevertheless, this model adequately responds to variation of the atmospheric conditions and may be used for determination of the soil moisture during the vegetation period between the wilting point and the fully saturated soil.

References

Choudhury, J. and *Idso B.*, 1985: An empirical model for stomatal resistance of field-grown wheat. *Agricultural and Forest Meteorology 36*, 65-82.

Denmead, O. and *Millar, B.*, 1976: Field studies of the conductance of wheat leaves and transpiration. *Agronomy Journal 68*, 307-311.

Fisher, M., Charles-Edwards, D. and *Ludlow M.*, 1981: An analysis of the effects of repeated short-term water deficits on stomatal conductance to carbon dioxide and leaf photosynthesis by the legume *Macroptilium atropurpureum* cv.Sirato. *Australian Journal of Plant Physiology 8*, 347-357.

Mitchurin, B., 1975: *Power of soil moisture* (in Russian). Gidrometeoizdat, Leningrad.

Roberts, J., Pymer, C., Wallace, J. and *Pitman, R.*, 1980: Seasonal changes in leaf area, stomatal and canopy conductances and transpiration from bracken below a forest canopy. *J. Applied Ecology 17*, 409-422.

Sirotenko, O., 1981: *Mathematical modelling of water-heat regime and crop productivity* (in Russian). Gidrometeoizdat, Leningrad.

Thompson, N., Barrie, I.A. and *Ayles, M.*, 1981: The Meteorological Office rainfall and evaporation calculation system. *Hydrological Memorandum*, No.45, England.

IDŐJÁRÁS

Quarterly Journal of the Hungarian Meteorological Service
Vol. 97, No. 1, January—March 1993

On the determination of vapour's molecular diffusion constant

F. Thoma

Consulting Engineer
Bimbó út 190/192, H-1026 Budapest, Hungary

(Manuscript received 17 December 1992; in final form 9 February 1993)

Abstract—In connection with the study of the individual characteristics of the water vapour's molecular diffusion constant D_m, which was published in the recent past (*Thoma*, 1991 b), some further questions may be arise. Accordingly, it is aimed to make clear that of the three parameters T_w (water temperature), T_a (air temperature) and R (relative humidity), respectively, which one is those having the greatest influence on the magnitude of D_m.

The author illustrates and analyses the effects of T_w as well as T_a on the molecular diffusion constant by the distribution function of $D_m = f(T_w)$ and $D_m = f(T_a)$, respectively. The effect of the relative humidity is still illustrated and analysed by the function of $D_m = f(R)$,—namely in the three cases of different water temperature, regarding four-four air temperatures for each case—i.e. by 3x4=12 function-curves, using a common system of co-ordinates.

Comparing the effects of different parameters one by one it seems that the magnitude of the relative humidity has the greatest influence on the magnitude of D_m above all. In the second place there may be mentioned the effect of the water temperature. The effect of the air temperature may be neglected.

Key-words: molecular diffusion constant, evaporating water surface, sprinkler irrigation.

1. Introduction

For the planning operations of the floating valve sheets (in the patent specification written as "coverplates") being used as an evaporation reduction apparatus (*Thoma*, 1967, 1971,1973, 1992), it is absolutely necessary to know, in the given case, the accurate value of the water-vapour's molecular diffusion constant D_m. (In this paper expression *molecular diffusion constant* is used because its values is rather constant compared to the turbulent diffusion coefficient, see *Thoma*, 1982.)

During the research work, have performed for long years, first the diffusion

constant's determination method has been developed (*Thoma*, 1982). On the basis of this method the functions of $D_m=f(T_w)$, $D_m=f(T_a)$ and $D_m=f(R)$ have been sketched out (*Thoma*, 1987). Hereupon, the individual characteristics of the molecular diffusion function of $D_m=f(T_w)$ have been analysed in detail (*Thoma*, 1991b).

From both theoretical and practical view points some further questions may be raised up. For example, of the three—in our opinion the most important—parameters, i.e. the water temperature T_w, the air temperature T_a and the relative humidity R, which one is that, having the greatest influence on the most-probable value of molecular diffusion constant $D_{m(m.p.)}$. It is thought that these questions may be answered correctly, first of all, by the application of distribution functions.

In the course of this study there will be presented:

(a) the distribution functions of the $D_m=f(T_w)$ and $D_m=f(T_a)$, using generally their values No. "n", in three-three cases; namely for the $D_m=f(T_w)$ function, when $T_a=16°C$ and 24°C, 30°C, respectively; and for the $D_m=f(T_a)$ function, when $T_w=16°C$, 24°C and 32°C, respectively,

(b) the linear functions of $D_m=f(R)$—using generally their values No."n" and No. "n_2"—to discuss the curves more precisely, similarly in three cases; namely when $T_w=16°C$, 24°C and 32°C, respectively.

Knowing these distribution functions and linear functions, we analyse the effects of the three most important parameters on the value of D_m functions. The investigations comprise the determination of values of the vapour's molecular diffusion constant, the magnitude of which depends on the air temperature and the evaporating water temperature between 0°C and 50°C (i.e. in the so called "middle range", *Thoma*, 1987, 1991b).

The aim of this study is to demonstrate the effect of the above mentioned parameters acting on the value of the molecular diffusion constant.

2. *Distribution function of vapour's molecular diffusion constant*

For the distribution function of vapour's molecular diffusion constant the normal, Gaussian distribution function has been adopted, which is defined (*Csoma* and *Szigyártó*, 1975) as

$$F(x) \equiv P(\xi<x) \equiv \Phi(x) = \frac{1}{\sigma\sqrt{2\pi}} \int_{-\infty}^{x} e^{-\frac{t-m}{2\sigma^2}} dt, \qquad (1)$$

where $F(x)$ is the distribution function, P the probability, ξ random variable, x

independent variable of the distribution function as well as of the empirical distribution function, $\Phi(x)$, σ standard deviation, σ^2 variance, m probable value.

The random variable ξ is, in the present case, equivalent the molecular diffusion constant. The undistorted estimation of variance of the sample-set is given by formula

$$\sigma^2 = \frac{\sum_{i=1}^{n} (x_i - \bar{x})^2}{n - 1}, \tag{2}$$

where n is the number of samples, x independent variable, $\bar{x}$ arithmetical mean of the independent variable.

The basic importance of the distribution originates from the thesis that the random variable ξ characterizing the phenomenon, may be written as a sum of several other ξ_i random variables

$$\xi^{(n)} = \xi_1 + \xi_2 + \ldots + \xi_n, \tag{3}$$

which will converge to the normal distribution,—in case of very common conditions—with the increase of the number of sample, symbolically

$$\lim_{n \to \infty} F(x)^{(n)} = \Phi x^{(n)}, \quad \text{if } x^{(n)} = \sum_{i=1}^{n} x_i. \tag{4}$$

The dependent variables belonging to the values of the different independent variables of this distribution function may be determined using the well known table by *Csoma* and *Szigyártó* (1975).

The table contains values of the distribution function $F(x)$ for the $x=x_t$ values in the region of $0 < x_t \leq 3$ with accuracy of 0.02, and in the region of $x_t > 3$ with accuracy of 0.2 under the conditions, $m=0$, $\sigma=1$, $x_t \geq 0$.

3. Individual characteristics of the distribution functions of vapour's molecular diffusion constant

3.1. Dependence on the evaporating water temperature

The first comparative, analytical examinations were carried out by distribution functions determined for three cases. The parameters, serving as starting-points, are summarized in *Table 1.*

Table 1. Parameters for the calculation of every single point of the three $D_m=f(T_w)$ functions as well as the values of the random variable $D_{m(m.p.)}$ (n is number of cases)

Individual cases	T_a	ΔT_a	R	T_w	n	$D_{m(m.p.)}$	$10^3\Delta D_{m(m.p.)}$
	°C	°C	%	°C		$cm^2\ s^{-1}$	$cm^2\ s^{-1}$
I	16		75	12-50	23	0,483	
		8					0,715
II	24		75	20-50	23	0,489	
		6					3,931
III	30		75	26-50	17	0,492	

As may be seen, the air temperature-differences ΔT_a—considering T_a as constant value for the individual cases—are close to each other, i.e. $\Delta T_a=8°C$ and 6°C, respectively. The relative humidity is, in all three cases, the same, i.e. $R=75\%$. The values of evaporating water temperatures—as the values of selected samples—were always chosen from the so called "working section" (by the number of specimen as : $n=23$, 23 and 17, respectively). In the last column of Table 1 the most probable values of the molecular diffusion constant are shown, which are deduced using the No. "n" molecular diffusion constant values of D_m given by equation

$$D_{m(m.p.)} = \frac{\sum D_m}{n}. \tag{5}$$

The values of $D_{m(m.p.)}$ are strikingly close to each other.

The three distribution functions are presented in *Fig. 1* using a common system of co-ordinates, in order to ensure the easier compatibility of the three distribution functions. The axis of abscissas represents the scale of the random variable, in this case, the values of the molecular diffusion constant, while the axis of ordinates represents the scale of the values of the empirical distribution function, at present, the values of $\Phi(x)=1-x$.

The three distribution functions show great similarity as it is expected. All the three curves may be characterized by strongly straddling bell-shaped curves. The bell-shaped curves and the places of their summits are located shifting to the right, in a very small degree, depending on the increasing air-temperature. These, relatively very small displacements mean that the air-temperature above the evaporating water surface has only small effect on the most probable value $D_{m(m.p.)}$ of the molecular diffusion constant (e.g. the increase of 8 °C and 6 °C,

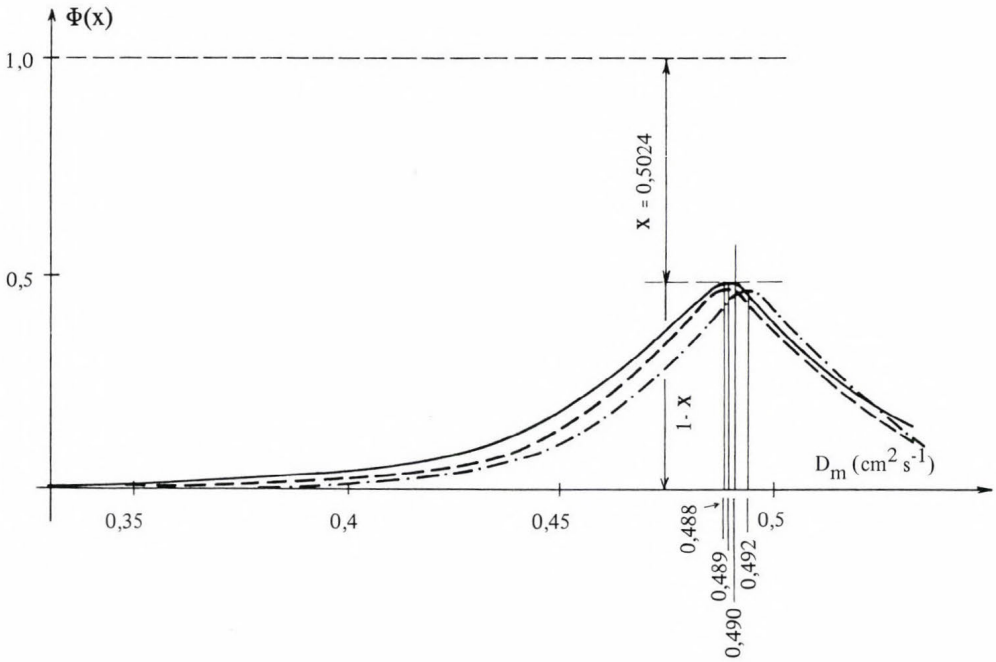

Fig. 1. Distribution functions of D_m as a function of T_w for different $T_a = 16°C$ (solid), 24°C (dashed) and 30°C (dot-dashed), respectively. The R is equal to 75% in all the three cases.

in the value of T_a will raise the value of $D_{m(m.p.)}$ by only 0,146% and 0,803%, respectively).

3.2. Dependence on the air temperature above the evaporating water surface

The next comparative, analytical examinations were carried out—similarly as in the Section 3—by distribution functions determined for the three cases. The values of parameters, serving as starting-points for calculation of $D_m = f(T_a)$ functions, are summarized in *Table 2*.

The water temperature differences ΔT_w—considering T_w as constant value for the individual cases—are equivalent, i.e. $\Delta T_w = 8°C$. Moreover, the relative humidities are, in all three cases, similarly equivalent, i.e. $R = 75\%$. While the values of air temperatures above the water, T_a —as the values of selected samples—are always chosen from the so called "working section" (by the number of specimen as $n = 21$, 23 and 23, respectively). In the last column of Table 2 there are shown the most probable values of the molecular diffusion constant which are deduced by using the No "n" molecular diffusion constant values of D_m as well as by the application of Eq. 5.

Table 2. Parameters for the calculation of every single point of the three $D_m = f(T_a)$ functions as well as the values of the random variable $D_{m(m.p.)}$ (n is number of cases)

Individual cases	T_w	ΔT_w	R	T_a	n	$D_{m-(m.p.)}$	$10^3 \Delta D_{m(m.p.)}$
	°C	°C	%	°C		$cm^2\ s^{-1}$	$cm^2\ s^{-1}$
I	16		75	0-20	21	0,460	
		8					17,103
II	24		75	6-28	23	0,477	
		8					12,702
III	32		75	14-36	23	0,489	

The three distribution functions are presented in *Fig. 2.* These distribution functions show also great similarity to those in Section 3. All the three curves are of bell-shaped similarly to Section 3.1. But here the right side of the curve is open from its half height downwards. The bellshaped curves and their culmination's points are shifting to the right (as compared with each others), in the same degree, depending on the increase of the water temperature. These relatively conspicuos displacements indicate how intense and determining is the effect of the evaporating water temperature on the most probable value $D_{m(m.p.)}$ of the molecular diffusion constant (e.g.: the increase of 8°C in the value of T_w will raise the value of $D_{m(m.p.)}$ by 3.7% and 2.7%, respectively).

Concerning the effect of T_w,—its determining character coming from above mentioned conclusion—it is reasonable to give a more detailed and correct explanation based on the mechanism of this physical phenomenon, showing which process produces this significant effect.

Earlier it has been mentioned (*Thoma*, 1974), that the water molecules, due to their kinetic energy in the evaporating water, are moving in different directions and with different velocity (Brownian/colloidal movement), depending on the actual water temperature. Some water molecules,—if their moving direction is perpendicular to the water surface—in case of suitable velocity, break through the pellicle of water surface influenced by the surface-tension and penetrate into the so called boundary layer next to the water surface (thickness of which equals to about 100 μm (*Katsaros et al.*, 1977).

It is well known that the colloidal-movement is proportional to the temperature of the elementary particles. The change of state between the water surface and boundary layer, intensifies in the case of increasing water temperature, as long as the boundary layer with the increased temperature will be

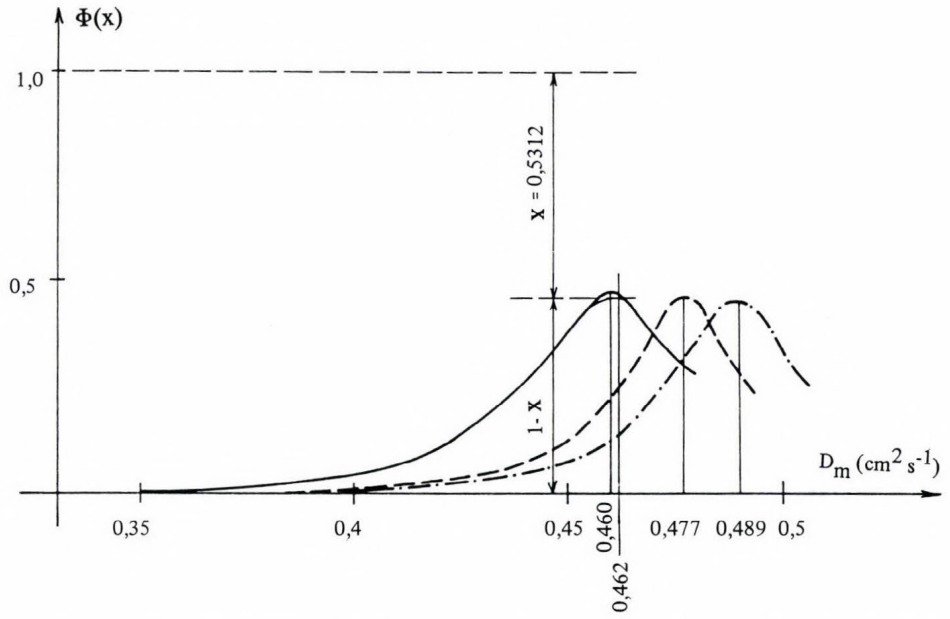

Fig. 2. Distribution functions of D_m as a function of T_a for different $T_w = 16°C$ (solid), 24°C (dashed) and 32°C (dot-dashed), respectively. The R is equal to 75% in all the three cases.

saturated again. This will induce a higher vapour-pressure in the boundary layer which leads to a higher vapour pressure difference as compared to the vapour pressure of the air layer being above the boundary layer. Consequently, the rate of molecular diffusion will increase between the two layers.

The distribution function's sample numbers "n" shown in Table 2 are near-by each others. While the relative humidity values of the air above the evaporating water having different temperatures T_a are equivalent (i.e. 75%) in each case. Thus, the shifting of the most probable value $D_{m(m.p.)}$ of the molecular diffusion constant is no doubt the consequence of change in the water temperature.

4. Individual characteristics of the functions $D_m = f(R)$ of vapour's molecular diffusion constant against the relative humidity of the air

4.1 Determination of the $D_m = f(R)$ curves

The investigations are based on three individual cases again, now instead of distribution functions simple function-groups are used. The parameters concerned are summarized in *Table 3*.

Table 3. Parameters used for the determination of individual points of the three function groups $D_m = f(R)$ and the values of molecular diffusion constants $D_{m(sing.)}$ of singular straights for different T_w, T_a and R.

Individual cases	T_w	T_a	R	n_1	n	n_2	$D_{m(sing)}$
	°C	°C	%	(left side)		(right side)	$cm^2\ s^{-1}$
		20,0	0- 75	4			
		19,0	0- 75	4			
		17,0	0- 93	6			
I	16	16,0	0-100		5		0,462
		15,8	0-100			4	
		15,4	0-100			5	
		13,0	0-100			5	
		10,0	0-100			5	
		27,0	0- 83	6			
		26,0	0- 85	4			
		25,0	0- 94	5			
II	24	24,0	0-100		5		0,475
		23,5	0-100			5	
		20,0	0-100			5	
		12,0	0-100			5	
		4,0	0-100			5	
		35,0	0- 80	5			
		34,0	0- 87	5			
		33,0	0- 93	6			
III	32	32,0	0-100		5		0,488
		31,8	0-100			6	
		31,4	0-100			5	
		30,0	0-100			5	
		29,0	0-100			5	

Three water temperatures (i.e. $T_w = 16$, 24 and 32°C) were associated with n_1+n+n_2 (generally $3+1+4$) and the air temperatures and the values of molecular diffusion coefficients were determined by an earlier introduced method (*Thoma*, 1987) for 4–6 different relative humidity data.

The pair of values, i.e. D_m against R obtained in this way are shown in *Fig. 3*. This figure is identical in principle but more detailed and complete as compared to the Fig. 1c of an earlier work published already in 1987 (*Thoma*, 1987). At that time we aimed merely to present the constructing possibility of the linear function R against D_m in case of different air temperatures, further, to draw some inferences.

In the present case Fig. 3 will give presumably several more interesting information which are taken into account below.

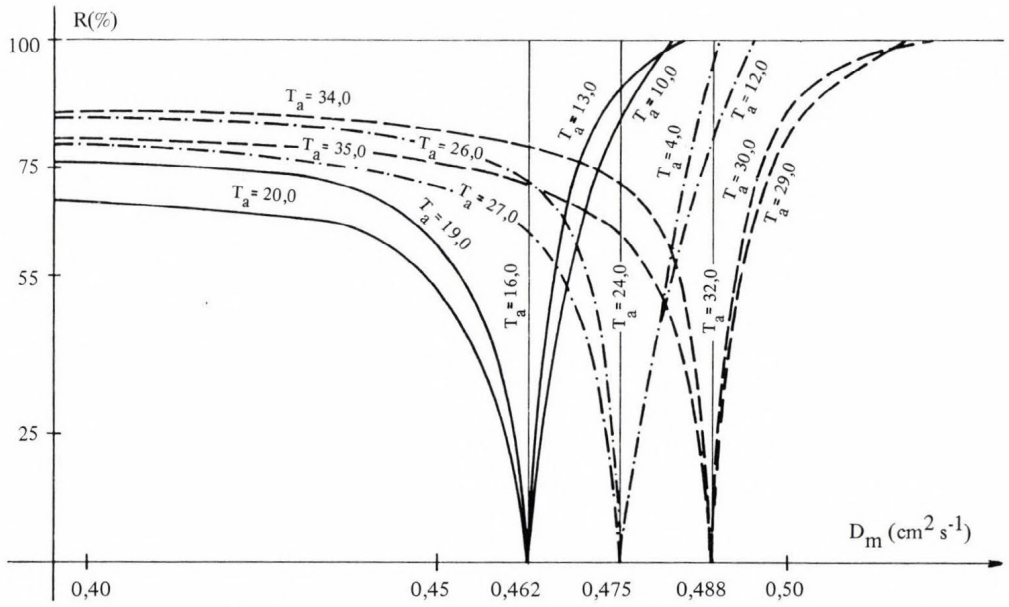

Fig. 3. Functions of D_m against R for different T_a (written on the curves) and $T_w = 16$°C (solid), 24°C (dot-dashed) and 32°C (dashed), respectively.

4.2 Individual characteristics of the $D_m = f(R)$ function curves

Analysing the function curves in Fig. 3, we have to notice three typical characters. To the water temperature's each fixed value (i.e. to $T_w = 16$, 24 and 32°C, respectively) two so-called "functiongroups" belong one of which opens on the left side and an other on the right side. Through the center of this function-group a vertical straight (a singular function-line) passes to which we shall refer later in more detailed. For example, selecting one of the function-group, to which the water temperature of $T_w = 24$ °C belongs, it may be seen that:

(1) If the function group located on the right side, i.e. when the water temperature, $T_w = 24$°C is fixed and the air temperatures are smaller than the fixed water temperature (i.e. $T_a = T_w - \Delta T$, and the curves belong to air temperatures of 23, 20 and 12°C, respectively), then it will be seen that the value of D_m does not increase uniformly with the increasing R value, but it increases in more and more degree.

However, as compared with the increase of the function-group being on the left side of the straight of the air temperature of $T_a = 24$°C the increasing is slow enough.

(2) On the contrary of the above statement if the water temperature is fixed, i.e. $T_w = 24$°C, and the function-group on the left of straight of the air

temperature of T_a=24°C is examined, (i.e. the $T_a=T_w+\Delta T$ curves, and T_a 26, 27 and 28°C, respectively), then it may be seen, that the value of D_m will decrease with the increase of the relative humidity not uniformly but in more and more degree.

However, as compared with the increase of the function-group on the right side of the straight of the air temperature of T_a=24°C the decreasing is slow enough.

This latter decrease takes place more rapidly than the increase mentioned in point 4.2(1) as it may be seen very well in Fig. 3.

4.3 Individual characteristics of the $D_{m(sing.)}$ singular straight in case of $T_w=T_a$

As an introduction it should be mentioned that the water temperature has always to be measured at the water surface because of the heat abstraction. According to the researches (*Katsaros*, 1977) the water temperature is higher by 1.0°C if measured at 0.5 cm below the water surface compared to the temperature measured immediately at the surface. This difference was determined by an experiment performed at 29°C water temperature.

During the designing of the function-lines it has been noticed that in case of $T_w=T_a$ the function's shape is a straight. This means that the same singular value of $D_{m(sing.)}$ belongs to any relative humidity values (e.g. in case of $T_w=T_a$=16°C the $D_{m(sing.)}$=0.462 cm^2 s^{-1}). Well then the question is how this is possible?

In order to answer this, let us adopt Eq. (4) in our recently published study concerning the value of vapour's molecular diffusion constant (*Thoma*, 1991 b):

$$D_m = k \frac{E(T_w) - RE(T_a)}{a(T_w) - Ra(T_a)}, \tag{6}$$

where D_m molecular diffusion constant (cm^{2}s^{-1}), k constant (4,633.10^{-7} s^{-1}), $E(T_w)$ vapour pressure of boundary layer (Hg mm), R relative humidity of the air (%), $E(T_a)$ air vapour pressure (Hg mm), $a(T_w)$ vapour concentration (g/cm^3), $a(T_a)$ air density (g/cm^3).

In our case—since the boundary layer's temperature (the vapour saturated layer's temperature) and the air layer's temperature above it are the same—the vapour pressure of $E(T_w)$ as well as $E(T_a)$ used in Eq. (6) are equivalent. Therefore, let us denote them generally by $E(T)$. For the vapour concentration the same situation is valid consequently its values will be denoted by $a(T)$.

Accordingly, the value of this special singular molecular diffusion constant will be as follows

$$D_{m(sing.)} = k \frac{E(T) - R \cdot E(T)}{a(T) - R \cdot a(T)}, \tag{7}$$

and after simplification

$$D_{m(sing.)} = k \frac{E(T)}{a(T)}, \tag{8}$$

which is after all visibly independent of the relative humidity and thus it assumes a fixed value indeed.

This value of $D_{m(sing.)}$ is a singular value for each temperature-pair of $T_w \equiv T_a$, and the function $D_{m(sing.)} = f(E(T)/a(T))$ belonging to them represents straights perpendicular to the axis of abscissas.

5. Possible practical application of the results

Drop and sprinkler irrigations are used all over the world. One of the most wide-spread irrigation method is the sprinkler-irrigation. But this has a drawback with regards to the drop-irrigation. Namely, the outcoming water (water drops, jet etc.) from the sprinkler-head suffer loss because of the evaporation before it reaches the soil. This is well known by the hydrologists (*Antal*, 1965). This loss is at least 30–40% which is more than has been supposed so far (generally 2–25%) which may be decreased in the future by selecting the right time and day's period, according to the present research.

Using meteorological forecastings there is given the possibility to choose the optimum irrigation period from the 24 hours of a day, based on $D_m = f(R)$ curves.

Accordingly, beside the temperature of the water sprinkled out from the head, which changes practically very small for 1 or 2 days it is possible to choose the most favorable air temperature and relative humidity in order to get the minimum value of the molecular or turbulent diffusion, $D_{m(min.)}$ or $D_{t(min.)}$. The optimum periods for irrigation will be most probably at the terms of dawn, sun-rise and at the beginning of night, after sunset.

6. Conclusions

(1) In case of constant air temperature and variable water temperature the curve of the molecular diffusion constant's distribution function is bell-shaped, ogival above and diverging underneath. The summits of these distribution curves, the most probable values of the molecular diffusion constant are located

very close to each other. It may be said that the air temperature does not influence the most probable value of the molecular diffusion constant considerably.

(2) In case of constant water temperature and variable air temperature the curve of the molecular diffusion constant's distribution function is bell-shaped, downward diverging at the top and defective in its right lower half. These distribution functions are shifting to the right considerably, depending on the increasing water temperature assumed to be constant value. Accordingly, the values of $D_{m(m.p.)}$ are increasing remarkably in the right direction. From these characteristics the conclusion can be drawn that the evaporating water temperature influences the most probable value of the molecular diffusion constant considerably.

(3) Comparing points (1) and (2), it can be stated that the water temperature has essentially higher effect on the value of the molecular diffusion constant than the air temperature does.

(4) In case of the functions $D_m=f(R)$, associating three constant water temperatures and variable air temperatures with them, the effect of relative humidity is relatively small on the molecular diffusion constant, in the section of $R=0$–55% it is nearly symmetrical to the left and right of the singular straight. But above 55% relative humidity, to the left of the singular straight the increase of the relative humidity has a rapidly decreasing effect on the molecular diffusion constant. At the same time to the right of the singular straight, the values of relative humidity above 55% increase the values of D_m but only in a moderate degree as compared to the case mentioned before.

(5) When examining the values of the distribution functions, it may be seen that the summits of independent variable x are found between the values of 0.5024 and 0.5312. This means a difference of cca. 5.42%. From this small difference a conclusion may be drawn that the choosing of the sample's number as well as the accuracy of the calculation method are correct enough.

(6) Among the functions of $D_m=f(R)$ there is a special one, namely when the two parameters, i.e. the values of temperatures T_w and T_a are equivalent. In this case the shape of the $D_m=f(R)$ function is straight vertical to the axis of abscissa, so called "singular straight". Accordingly, one singular straight belongs to each $T_w=T_a$ temperature-pair which is independent of the relative humidity.

(7) The conclusion from points 1–6 indicates that the relative humidity plays so important role in the formation of the value of the molecular diffusion constant. This effect of the relative humidity is larger as compared to that of temperatures T_w or T_a.

(8) The saturated "air cushion" mentioned in the English Patent (*Thoma*, 1971) and the physical explanation of the cushion's development formulated earlier (*Thoma*, 1980) demonstrate the primary effect of R as well. Namely, in connection with the vapour hydraulic theory of different valve sheets it came

to light that assuming the relative humidity of the air to be $R=40\%$ the relative humidity $R_{thicked}$ of the artifically thicked air-layer between the valve-sheet and the evaporating water surface, increased by the following degree:

(a) in case of rectangular valve sheet and reducing the evaporation by 84% the $R_{thicked}=95\%$ (*Thoma*, 1989),

(b) in case of triangle-formed valve sheet and reducing the evaporation by 79%, the $R_{thicked}=98\%$ (*Thoma*, 1991a).

(9) Similarly to the curves outlined in Fig. 3., there may be drawn further innumerable function-groups of $D_m=f(R)$. Based on these function groups we can choose the time-table for sprinkler-irrigation taking into consideration the evaporation loss of delivered irrigation water in a more economically way (*Dobos*, 1992, personal consultation).

The values of the air temperature and relative humidity are predicted for several days by the meteorological services (*Antal*, 1992, personal consultation).

References

Antal, E., 1965: Irrigation and meteorology (in Hungarian). *Időjárás 69*, 248-257.

Csoma, J. and *Szigyártó, Z.*, 1975: *Adoption of mathematical statistics in hydrorlogy* (in Hungarian). VITUKI publication Budapest, 1-220.

Katsaros, K., Liu, W. Businger, T. Joost, A. and *Tillman, J. E.*, 1977: Heat transport and thermal structure in the international boundary layer measured in an open tank of water in turbulent free convention. *J. Fluid Mech. 83*, Part 2, 311-335.

Thoma, F., 1967: Evaporation model tests (in Hungarian). *Hidrológiai Tájékoztató*, November, 34-41.

Thoma, F., 1971: Apparatus for Reducing Evaporation from a Liquid Surface. No. 1, 229 852, The Patent Office, London, Filed 22 May 1968, 1-3.

Thoma, F., 1973: Model tests with thin sheets to reduce evaporation. *J. of the Irrigation and Drainage Division*, ASCE, *Vol. 99*, No. IR 2, Proc. Paper 9779, June, 1973, 117-131.

Thoma, F., 1974: Property of vapour's elementary particles originating at vaporization (in Hungarian). *Hidrorlógiai Tájékoztató*, 40-44.

Thoma, F., 1980: Motion of vapour and the forcess inducing of that (in Hungarian). *Hidrológiai Tájékoztató*, October, 14-15.

Thoma, F., 1982: Vapour's diffusion constant and its numerical determination (in Hungarian). *Hidrológiai Tájékoztató*, October, 6-9.

Thoma, F., 1987: Function of vapour's diffusion constant and its Gaussian-distribution (in Hungarian). *Hidrológiai Tájékoztató*, April, 15-18.

Thoma, F., 1989: Numerical determination of on one or on two oposite sides open rectangle-formed sheet's characteristic--curve, in case of meteorological circumstances given in advance (in Hungarian). *Hidrológiai Tájékoztató*, October, 22-25.

Thoma, F., 1991a: Numerical determination of on one or two sides open equilateral

triangle-formed sheet's characteristic-curve, in case of meteorlological circumstances given in advance (in Hungarian). *Hidrológiai Tájékoztató*, April, 37-39.

Thoma, F., 1991b: Individual characteristics of the vapour molecular diffusion function (in Hungarian). *Időjárás 95*, 245-257.

Thoma, F., 1992: Evaporation Reduction with Floating Sheets. International Commission on Irrigation and Drainage. *Proc. of the Rapport of the 16th European Regional Conference*, 21-27 June, Budapest. Vol. I. Drough Phenomena, 501-515.

BOOK REVIEW

F. Fliri: **The Snow in North- and East-Tyrol 1895–1991** (in German). Universitätsverlag Wagner, Innsbruck, 1992 (Vol. I: pp. 593, Vol. II: pp. 553).

As a climatologist–retired since 1977–and an old-timer researcher of the snow conditions of Hungary, I took this work in my hand with a great deal of genuine interest.

The title and the size of the two volumes already gave me an advance hint of the level of detail, and rightly so. *Most probably no one in the worlds has ever produced such an exhausting and carefully prepared monography about the snow cover of a relatively small area.*

The two volumes comprise the observations of snow conditions carried out at 80 stations all over *North-, Central-* and *East-Tyrol*, through a period of nearly 100 years. Among the 80 stations there were 44 with observations from 1895 onwards, with only minor gaps (at 20 stations) during World Wars I and (particularly) II. From 1950 onwards the observation series are uninterrupted at all of the 80 stations.

Firstly a short, general historical overview is given about snow observations in Tyrol. Then, following some statistical information about the observation network, the *average snow cover data* are presented in figures and diagrams.

Next, a particularly interesting part deals with *snow cover data in summer*, from 65 stations. Between altitudes of 490 and 1950 metres above sea level, snow cover–as we see–is a familiar phenomenon in the May–June and September–October periods. Above 1000 metres an unbroken snow cover is a relatively frequent–although not very long-lived–phenomenon.

For the 95 winters between 1895 and 1991, a graphical presentation is given of snow cowers deeper than 1 cm (these figures may be called: "snow assurances"). Next, we find tabulations of dates marked with maximum snow depths, showing that below 2000 metres these maxima occur in February, while above 2000 metres in March.

The most voluminous part of the work contains the *chronological diagrams* of snow depths. This part of the work is the novelty of the whole monography. The presentation is very instructive. The snow cover builds up before our eyes–like in a movie–, reaches its maximum depth, and then–more slowly–it recedes. It is experimental to follow the story of 95 winters in the light of these snow cover data. Watching the unfolding story of snow in Austria, as it is presented in Professor Fliri's work, this Hungarian reviewer can only admire the substance (namely the snow), which has become one of the great assets of Austrian tourist industry in our age.

M. Kéry

ATMOSPHERIC ENVIRONMENT

an international journal

To promote the distribution of Atmospheric Environment *Időjárás* publishes regularly the *contents* of this important journal. For further information the interested reader is asked to contact *Dr. P. Brimblecombe,* School for Environmental Sciences, University of East Anglia, Norwich NR 7TJ, U.K.

Volume 26A Number 16 1992

Volume 26A Number 17 1992

R.I. Sykes and *D.S. Henn*: Large-eddy simulation of concentration fluctuations in a dispersing plume, 3127-3144.

D.S. Henn and *R.I. Sykes*: Large-eddy simulation of dispersion in the convective boundary layer, 3145-3159.

K. Ruoss, R. Dlugi, C. Weigl and *G. Hänel*: Intercomparison of different aethalometers with an absorption technique: laboratory calibrations and field measurements, 3161-3168.

D. Knotková and *K. Barton*: Effects of acid deposition on corrosion of metals, 3169-3177.

G.H.L. Verver and *F.A.A.M. De Leeuw*: An operational puff dispersion model, 3179-3193.

A. Bytnerowicz, P.J. Dawson, C.L. Morrison and *M.P. Poe*: Atmospheric dry deposition on pines in the Eastern Brook Lake Watershed, Sierra Nevada, California, 3195-3201.

A.S. Mason and *F.A. Gifford*: Atmospheric tracer dispersion over a 24-h time span, 3203-3205.

G. Hacisalihoglu, F. Eliyakut, I. Olmez, T.I. Balkas and *G. Tuncel*: Chemical composition of particles in the Black Sea atmosphere, 3207-3218.

R. Mathur, L.K. Peters and *R.D. Saylor*: Sub-grid representation of emission source clusters in regional air quality modeling, 3219-3238.

Volume 26A Number 18 1992

R. Kozlowski, A. Hejda, S. Cęckiewicz and *J. Haber*: Influence of water contained in porous limestone on corrosion, 3241-3248.

M. Bennett, S. Sutton and *D.R.C. Gardiner*: An analysis of Lidar measurements of buoyant plume rise and dispersion at five power stations, 3249-3263.

M. Luria, J.F. Boatman, D.L. Wellman, R.L. Gunter, B.A. Watkins, S.W. Wilkison and *C.C. Van Valin*: Lake Michigan Ozone Study (LMOS): measurements from an instrumented aircraft, 3265-3277.

D. Grosjean: Formic acid and acetic acid: emissions, atmospheric formation and dry deposition at two southern California locations, 3279-3286.

A. Leonardi, H. Burtscher and *H.C. Siegmann*: Size-dependent measurement of aerosol photoemission from particles in diesel exhaust, 3287-3290.

R.S. Hamilton and *T.A. Mansfield*: The soiling of materials in the ambient atmosphere, 3291-3296.

C. Sabbioni and *G. Zappia*: Characterization of particles emitted by domestic heating units fueled by distilled oil, 3297-3304.

X.Q. Zhang and *P.H. McMurry*: Evaporative losses of fine particulate nitrates during sampling, 3305-3312.

F.O. Hoffman, K.M. Thiessen, M.L. Frank and *B.G. Blaylock*: Quantification of the interception and initial retention of radioactive contaminants deposited on pasture grass by simulated rain, 3313-3321.

T.C. Haas: Redesigning continental-scale monitoring networks, 3323-3333.

J.C. Chow, J.G. Watson, D.H. Lowenthal, P.A. Solomon, K.L. Magliano, S.D. Ziman and *L.W. Richards*: PM10 source apportionment in California's San Joaquin Valley, 3335-3354.

J. Alcamo, J. Bartnicki, K. Olendrzński and *J. Pacyna*: Computing heavy metals in Europe's atmosphere—I. Model development and testing, 3355-3369.

Volume 27A Number 1 1993

D.H.F. Atkins and *D.S. Lee*: Indoor concentrations of ammonia and the potential contribution of humans to atmospheric budgets, 1-7.

A.-L. Pasanen, M. Nikulin, M. Tuomainen, S. Berg, P. Parikka and *E.-L. Hintikka*: Laboratory experiments on membrane filter sampling of airborne mycotoxins produced by *Stachybotrys atra* Corda, 9-13.

Liu Yangang: Statistical theory of the Marshall-Palmer distribution of raindrops, 15-19.

A.P. Altshuller: Production of aldehydes as primary emissions and from secondary atmospheric reactions of alkenes and alkanes during the night and early morning hours, 21-32.

J. Collett Jr, B. Oberholzer and *J. Staehelin*: Cloud chemistry at Mt Rigi, Switzerland: dependence on drop size and relationship to precipitation chemistry, 33-42.

G.P.J. Draaijers and *J.W. Erisman*: Atmosperic sulphur deposition to forest stands: throughfall estimates compared to estimates from inference, 43-55.

K.H. Becker, J. Bechara and *K.J. Brockmann*: Studies on the formation of H_2O_2 in the ozonolysis of alkenes, 57-61.

F. van den Berg: Measured and computed concentrations of methyl isothiocyanate in the air around fumigated fields, 63-71.

D. Weihs and *R.D. Small*: An approximate model of atmospheric plumes produced by large area fires, 73-82.

L. Camarero and *J. Catalan*: Chemistry of bulk precipitation in the central and eastern Pyrenees, northeast Spain, 83-94.

M.S. El-Shobokshy and *Y. G. Al-Saedi*: The impact of the Gulf war on the Arabian environment–I. Particulate pollution and reduction of solar irradiance, 95-108.

Technical Notes

H. Sauren, E. Gerkema, D. Bićanić and *H. Jalink*: Real-time and *in situ* detremination of ammonia

Volume 27A Number 2 1993

Volume 27A Number 3 1993

First Ibero-American Conference on the Atmospheric Environment, CIAMAA91/IACAE91

NOTES TO CONTRIBUTORS

The purpose of *Időjárás* is to publish papers in the field of theoretical and applied meteorology. These may be reports on new results of scientific investigations, critical review articles summarizing current problems in certain subject, or shorter contributions dealing with a specific question. Authors may be of any nationality but papers are published only in English.

Papers will be subjected to constructive criticism by unidentified referees.

* * *

The manuscript should meet the following formal requirements:

Title should contain the title of the paper, the names(s) of the author(s) with indication of the name and address of employment.

The title should be followed by an *abstract* containing the aim, method and conclusions of the scientific investigation. After the abstract, the *key-words* of the content of the paper must be given.

Three copies of the manuscript, typed with double space, should be sent to the Editor-in-Chief: *P.O. Box 39, H-1675 Budapest,* Hungary.

References: The text citation should contain the name(s) of the author(s) in Italic letter or underlined and the year of publication. In case of one author: *Miller* (1989), or if the name of the author cannot be fitted into the text: *(Miller,* 1989); in the case of two authors: *Gamov* and *Cleveland* (1973); if there are more than two authors: *Smith et al.* (1990). When referring to several papers published in the same year by the same author, the year of publication should be followed by letters a,b etc. At the end of the paper the list of references should be arranged alphabetically. For an article: the name(s) of author(s) in Italics or underlined, year, title of article, name of journal, volume number (the latter two in Italics or underlined) and pages. E.g. *Nathan, K. K.,* 1986: A note on the relationship between photosynthetically active radiation and cloud amount. *Időjárás 90,* 10-13. For a book: the name(s) of author(s), year, title of the book (all in Italics or underlined with except of the year), publisher and place of publication. E.g. *Junge, C. E.,* 1963: *Air Chemistry and Radioactivity.* Academic Press, New York and London.

Figures should be prepared entirely in black India ink upon transparent paper or copied by a good quality copier. A series of figures should be attached to each copy of the manuscript. The legends of figures should be given on a separate sheet. Photographs of good quality may be provided in black and white.

Tables should be marked by Arabic numbers and provided on separate sheets together with relevant captions. In one table the column number is maximum 13 if possible. One column should not contain more than five characters.

Mathematical formulas and *symbols:* non-Latin letters and hand-written marks should be explained by making marginal notes in pencil.

The final text should be submitted both in manuscript form and on *diskette.* Use standard 3.5" or 5.25" DOS formatted diskettes for this purpose. The following word processors are supported: WordPerfect 5.1, WordPerfect for Windows 5.1, Microsoft Word 5.5, Microsoft Word for Windows 2.0. In all other cases the preferred text format is ASCII.

* * *

Authors receive 30 *reprints* free of charge. Additional reprints may be ordered at the authors' expense when sending back the proofs to the Editorial Office.

Published by the Hungarian Meteorological Service

Budapest, Hungary

INDEX: 26 361

HU ISSN 0324-6329